



“Soft” Alkali Bromide and Iodide Fluxes for Crystal Growth

Vladislav V. Klepov*, Christian A. Juillerat, Kristen A. Pace, Gregory Morrison and Hans-Conrad zur Loye*

Department of Chemistry and Biochemistry, University of South Carolina, Columbia, SC, United States

OPEN ACCESS

Edited by:

Soumyajit Roy,
Indian Institute of Science Education
and Research Kolkata, India

Reviewed by:

Changui Lin,
Ningbo University, China
Malla Reddy Chilla,
Indian Institute of Science Education
and Research Kolkata, India

*Correspondence:

Vladislav V. Klepov
klepov@mailbox.sc.edu
Hans-Conrad zur Loye
zurloye@mailbox.sc.edu

Specialty section:

This article was submitted to
Inorganic Chemistry,
a section of the journal
Frontiers in Chemistry

Received: 20 October 2019

Accepted: 19 May 2020

Published: 26 June 2020

Citation:

Klepov VV, Juillerat CA, Pace KA,
Morrison G and zur Loye H-C (2020)
“Soft” Alkali Bromide and Iodide
Fluxes for Crystal Growth.
Front. Chem. 8:518.
doi: 10.3389/fchem.2020.00518

In this review we discuss general trends in the use of alkali bromide and iodide (ABI) fluxes for exploratory crystal growth. The ABI fluxes are ionic solution fluxes at moderate to high temperatures, 207 to ~1,300°C, which offer a good degree of flexibility in the selection of the temperature profile and solubility. Although their main use is to dissolve and recrystallize “soft” species such as chalcogenides, many compositions with “hard” anions, including oxides and nitrides, have been obtained from the ABI fluxes, highlighting their unique versatility. ABI fluxes can serve to provide a reaction and crystallization medium for different types of starting materials, mostly the elemental and binary compounds. As the use of alkali halide fluxes creates an excess of the alkali cations, these fluxes are often reactive, incorporating one of its components to the final compositions, although some examples of non-reactive ABI fluxes are known.

Keywords: flux crystal growth, alkali halide fluxes, chalcogenides, single crystals, inorganic synthesis

INTRODUCTION

Crystal growth from solution rests on the well-known principle of supersaturation that can be controlled by many factors, such as the solvent nature, polarity, temperature, competing compounds present in the solution, etc. All these parameters can be finely optimized to achieve the formation of good quality crystals, which are necessary for the structural characterization via single crystal X-ray diffraction of a new compound (Kanatidis and Sutorik, 1995). Solution crystal growth in different organic solvents works well for most organic compounds; however, crystallization of non-ionic extended structures is more challenging and a far less understood process. While ionic compounds and complexes can be easily recrystallized from a polar solvent, such as water or acetonitrile, at room or slightly elevated temperature, more covalent extended structures can only be obtained under conditions when the system has enough energy to overcome the energetic barriers related to breaking and recombination of covalent bonds. Although water can still be employed for crystallization at high temperatures (and often is), preventing water evaporation from a reaction vessel becomes increasingly difficult above ~220–230°C, a temperature at which polytetrafluoroethylene (PTFE) softens and standard hydrothermal techniques can no longer be used. Beyond this temperature, a much more sophisticated apparatus has to be used to be able to use water and other common solvents as a reaction media (Pace et al., 2018).

A convenient alternative to conventional solvents is various inorganic compounds that melt at readily achievable temperatures without reaching their boiling points during the reaction, circumventing the necessity of having expensive closed reaction vessels that can withstand high pressures. One well-known example of a high temperature flux is MoO₃, which has been widely used for crystallizing various phases, for example, uranium oxides (Juillerat et al., 2019). This compound melts at 795°C, creating a reaction and crystallization medium for the starting

materials, and can be slowly evaporated to promote the formation of large single crystals by slow oversaturation of the solution. Another major benefit of using fluxes for crystal growth is the ability to assume a kinetic control over a reaction. High temperature solid state reactions are often carried out at temperatures above 600°C to achieve sufficient diffusion rates. A downside of using high temperatures is the inevitable formation of thermodynamic stable products commonly observed with rather simple binary or ternary compositions (Kanatidis and Sutorik, 1995). The use of a flux allows for circumventing this limitation as a molten, liquid flux component significantly improves diffusion rates of a reaction by solubilizing the starting materials and therefore products can be obtained at lower temperatures and shorter reaction times. This offers an additional degree of control of the reaction conditions, paving a path toward kinetic products.

There are a number of excellent reviews devoted to flux crystal growth in general (Kanatidis and Sutorik, 1995; Bugaris and zur Loye, 2012; Liu et al., 2013), the use of selected fluxes (Kanatidis et al., 2005; Kanatidis, 2017), and materials that can be obtained using fluxes (Bugaris and Ibers, 2010). Chloride fluxes are among the most universal and widely applied fluxes, and have been extensively used for crystallization of oxides, chalcogenides, and chlorides (Bugaris and zur Loye, 2012). Their heavier counterparts, bromide and iodide fluxes, have attracted much less attention, although they offer a wider reaction temperature range. In this review, we focused on alkali bromide and iodide (ABI) fluxes to summarize and rationalize their application in exploratory crystal growth. We show their application to different systems to reveal most often used approaches and highlight possible future directions in the development of the alkali bromide and iodide flux technique.

GENERAL CONSIDERATIONS

The most important factor that governs processes during flux crystal growth is supersaturation. Ideally, once the starting materials have dissolved in a flux at a peak temperature, the supersaturation is reached when the concentration of the products exceeds their solubility upon decreasing temperature. After crossing the saturation limit, the melt becomes oversaturated and the nucleation process, which usually takes place on the walls of the reaction vessel or the surface of the melt, occurs more rapidly than nuclei dissolution, resulting in some of the nuclei reaching their critical size to become seed crystals that initiate the crystal growth process. According to the classical view on crystal growth, the size of the crystals is a function of how fast the oversaturation occurs, the growth of larger crystals is promoted by slower oversaturation, which favors the growth process over nucleation, while the opposite result, a large number of smaller crystals, can be achieved by rapid oversaturation of the melt. Although there are two dominating factors that affect the rate at which the melt is oversaturated, temperature profile, and the nature of the flux, other factors, such as crucible size and material, have been recently realized as

having a great impact on the products of a flux reaction and will be discussed in more detail in the following sections.

Starting Materials

In order to successfully carry out a flux reaction one must carefully select appropriate starting materials, a flux component, a reaction vessel, and a temperature profile. The starting reagents are most commonly considered first since they largely control the composition of the target product, a flux must be then chosen to dissolve the chosen reactants, a reaction vessel must be chosen that will successfully contain the flux, and lastly a temperature profile must be picked that supports all three of the previous choices.

There are several common approaches to choosing starting materials which include recrystallizing a polycrystalline precursor, reaction of the elements, and binary reagents, although starting material selection is oftentimes a matter of reagent availability. Often, a polycrystalline sample of the desired product (precursor) can be obtained easily by other methods, typically by solid state methods, and then recrystallized in a flux to obtain a single crystalline product (Zeng et al., 2008). In this approach, the choice of flux is essential, as the flux should dissolve the starting material in order to aid in the crystallization; however, the flux must not form stable compounds with the components of the precursor, which is often difficult to achieve since the solvent must break the covalent bonds of the precursor. It is hard to predict which flux will be suitable for this role, especially for alkali halide fluxes, as they contain alkali metal cations that readily incorporate into the final products. More often, different fluxes are probed for suitability for a certain system, as it happens with selection of an organic solvent for organic systems.

Other approaches use fluxes both as a reactant and crystallization medium at the same time. One such approach involves the use of elements as starting materials and has proved useful for the precise control over the reaction composition in a closed system. The downside of using some of the elements is their volatility and difficulties with handling hazardous substances. For example, the use of chlorine or bromine is rather limited in closed systems, such as evacuated fused silica tubes, while chloride/bromide fluxes can offer a safe and convenient source of chlorine/bromine (Ruck and Schmidt, 2003; Yahia et al., 2010; Cortese et al., 2015; Read et al., 2015). Sulfur is another example and has been used in the elemental form in many reactions, although it has a boiling point of ~445°C and builds up pressure beyond this temperature, potentially resulting in tube bursting. To prevent this, longer ramping times are required which allow the starting materials to react with each other, forming non-volatile species. This disadvantage can be overcome by using binary compounds, which circumvents the use of elemental sulfur and reduces the reaction time without a significant risk of tube bursting. The use of binaries is especially efficient for exploratory crystal growth as it offers fast screening of phase space and identification of stable compositions. The downside of using the binary compounds is the occasional difficulty of obtaining binary phases that are not commercially available or binary starting reagents that

contain unexpected impurities that alter the outcome of the reaction, with product formation depending on the reagent's lot (Wells et al., 2010). For example, rare earth sulfides are not currently commercially available, except for lanthanum sulfide, and require additional experiments to obtain the pure starting materials (Klepov et al., 2019a).

Recrystallization of materials that were obtained via the solid state route and reactions between elements or binaries are by far the most popular reactions employing fluxes. There are some interesting approaches that are not widely employed, but offer an alternative way of synthesis, which sometimes can save a lot of efforts. For example, Guo, Huang, and coworkers use oxides accompanied by elemental sulfur and elemental boron to obtain sulfide phases (Guo et al., 2009). Boron has a high affinity for oxygen, attacking oxides to form B_2O_3 that causes the reaction, which is accompanied by the reduction of sulfur to sulfide, to form a sulfide *in situ*. Coupled with a flux that promotes the reaction and then crystal growth, this approach offers a convenient way for exploratory crystal growth as it allows for using oxides, which usually are more readily available than sulfides or the elements. Another approach is oxidative elimination in the presence of NaI/CsI flux that has recently been employed by Woo et al. (2019). In this reaction, CuI was used as an oxidizer to create an oxidized boron phosphide Na_2BP_2 according to the reaction $Na_3BP_2 + CuI \rightarrow Na_2BP_2 + Cu + NaI$. This work is a nice illustration of a precise control over the reaction conditions, guided by PXRD, to form a desired species.

Unlike a solid state reaction, which offers the final product in, ideally, pure form at the end of a reaction, flux crystal growth involves one crucial step after the reaction is done—separation of residual flux from the products. For ABI fluxes, most of the common polar solvents serve this purpose well. Although water is the most common choice to dissolve a flux, most of the products obtained via ABI flux crystal growth are air- or moisture-sensitive, which requires the use of anhydrous organic solvents, such as methanol, ethanol, or DMF. These solvents offer a relatively fast, within hours, removal of a residual flux, with little damage to moisture sensitive crystals. Additional precautions should be taken with air sensitive crystals, and properly degassed and dehydrated solvents should be used.

Reaction Vessels

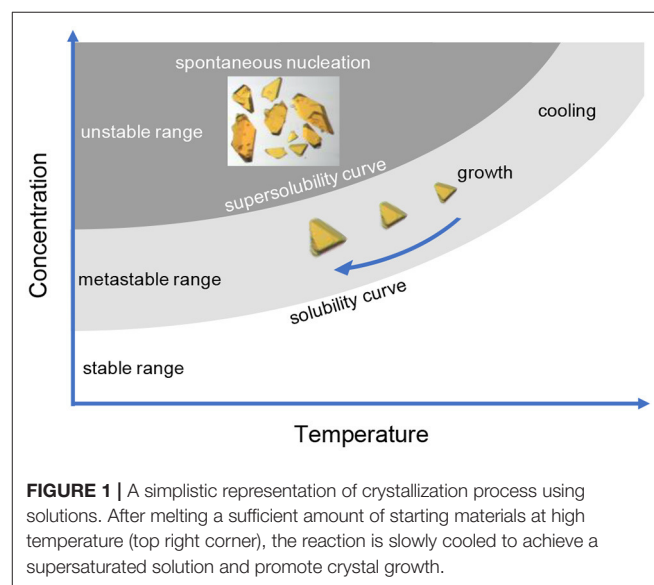
Compatibility between the reaction vessel and the flux is among the most important criteria for choosing a reaction vessel. While ABI fluxes are largely compatible with almost any reaction vessel of choice, using a mixed flux that includes a fluoride component will limit the available choices, as fluorides tend to extensively attack fused silica and alumina reaction vessels. Although fluoride fluxes are incompatible with alumina, small amounts of metal fluorides can be tolerated without debilitating damage to the vessel. Some of the syntheses reported for ABI fluxes use metal fluoride starting materials, specifically Schleid's work, and carbon coating the tube, or containing the reaction in an alumina crucible or gold ampule and using the fused silica as secondary containment proved successful in protecting the fused silica tube from the small amount of metal fluoride. Although ABI fluxes are generally considered compatible with fused silica tubes, there are reports on using a bromide flux in a fused silica

tube that resulted in Si incorporation from the tube (Lipp et al., 2012). This can be limited by the use of carbon coating, or a secondary container.

Other important factors for choosing reaction vessels are the desired atmosphere, the melting point, and in some cases the surface to volume ratios. Reaction vessels open to atmosphere, for example alumina and platinum crucibles, are primarily used for oxide synthesis, as targeted synthesis of halide, chalcogenide, and pnictide products often limit the amount of oxygen available to the reaction. Evacuated and sealed fused silica and Pyrex tubes can be used for closed systems, where fused silica has a much higher melting point and is more frequently used than Pyrex. The synthesis of the reported chalcogenides, oxychalcogenides, and pnictides, are almost exclusively carried out in evacuated fused silica tubes to exercise control over the incorporation of oxygen. In contrast, many different reaction vessels were used for halide containing products, including open alumina and platinum reaction vessels and sealed fused silica tubes. Additionally, several reported syntheses used He arc-sealed tantalum or niobium ampules. Although not discussed in any ABI flux papers, the surface area to volume ratio of the reaction vessels has been found to play a significant role in alkali chloride/fluoride flux reactions and could be important to consider in further studies using ABI fluxes (Morrison et al., 2016a).

Temperature Profiles

For crystal growth to occur, a solution must be sufficiently supersaturated to facilitate nucleation. In molten solutions, it is important to select a flux that is capable of dissolving the reactants and has a substantial change in solubility over the temperature range of interest, otherwise, the nucleated crystals will be re-dissolved and no single crystals will form. The optimal rate of nucleation occurs over a given temperature range which is specific to each system, thus exploratory crystal growth largely focuses on this determination (Figure 1; Bugaris and zur Loye, 2012; Juillerat et al., 2019).



Indeed, selecting an appropriate reaction temperature is among the most critical considerations to make when conducting crystal growth experiments. ABI fluxes offer a great deal of versatility when it comes to accessible temperature ranges, and have generally been used over a wide temperature range from ~400 to 1,000°C. The melting points of the ABI fluxes and some selected eutectics are listed in **Table 1**. An extremely helpful tool

in flux selection is the FactSage thermochemical database, which offers a large number of binary salt phase diagrams with the compositions and melting points of eutectic mixtures (Bale et al., 2002, 2009, 2016). **Figure 2** shows the temperature ranges used most frequently for the compounds discussed in this review, and demonstrates that reactions involving ABI fluxes have typically been carried out at temperatures 50–200°C higher than the melting point of the flux. There are many examples that indicate a significant influence of the reaction temperature on the resulting crystal morphology; for example, lower temperatures may produce irregularly-shaped crystals while increasing temperature may favor more defined morphologies.

One important feature of alkali iodide fluxes is their ability to build up pressure of iodine upon heating to high temperatures. This feature can be illustrated by a recent report by Winiarski et al., in which solid state incorporation of CsCl, CsBr, and CsI into $\text{Cu}_5\text{O}_2(\text{PO}_4)_2$ was carried out to achieve the formation of the $(\text{CsX})\text{Cu}_5\text{O}_2(\text{PO}_4)_2$ ($X = \text{Cl}, \text{Br}, \text{and I}$) salt inclusion

TABLE 1 | Melting point of alkali bromide and iodide fluxes and some eutectics with low melting points.

Salt	m.p., °C	Salt	m.p., °C	Mixtures, molar ratio	m.p., °C
LiBr	552	LiI	469	CsI/LiI (34:66)	~207
NaBr	747	NaI	661	KI/LiI (63:37)	~286
KBr	734	KI	681	CsBr/LiBr(37:63)	~281
RbBr	693	RbI	642	NaI/CsI (49:51)	~420
CsBr	636	CsI	621	CsBr/NaBr (58:42)	~458

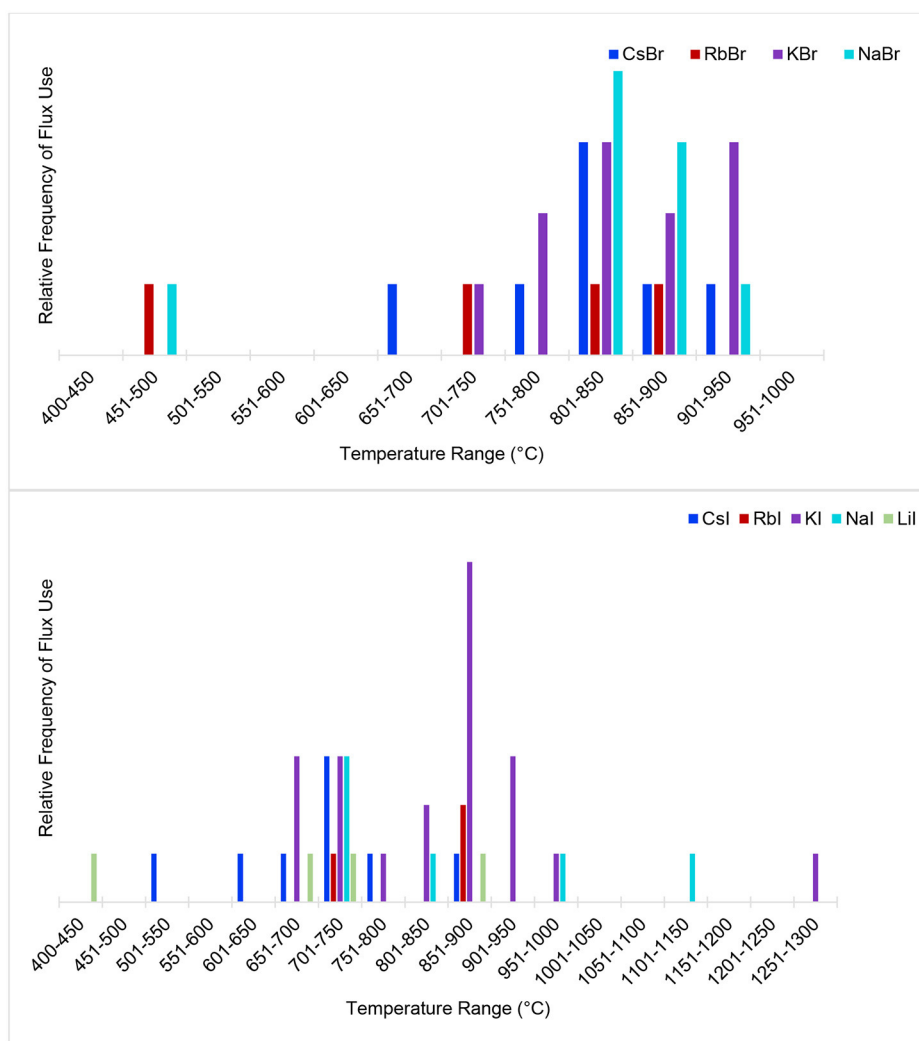


FIGURE 2 | Flux temperature ranges that have been used to obtain the compounds discussed in this review.

phases (Winiarski et al., 2019). While CsCl and CsBr can be obtained by quenching a solid state reaction between the respective alkali halide salt and $\text{Cu}_5\text{O}_2(\text{PO}_4)_2$, the iodide analog was obtained by slow cooling to equilibrate the iodine vapors with the sample. The presence of water vapor can increase the amount of iodine formed via the reaction: $\text{CsI} + \text{H}_2\text{O} \rightarrow \text{CsOH} + \text{HI}$, with subsequent decomposition of HI to the elements (Gouëlle et al., 2018). Considerable work has been carried out to study the thermal behavior of CsI due to the presence of radioactive iodine and cesium, present as CsI in nuclear reactors (Gouëlle et al., 2018).

There has also been a wide range of reaction dwelling times reported for ABI fluxes, ranging from no dwell to dwell periods of up to 5 weeks. In general, there does not seem to be much correlation between the flux used and the selected dwell times, though in many cases, increasing dwell times results in larger crystals. Similarly, cooling rates of $\sim 1\text{--}20^\circ\text{C}$ per hour over a range of about $200\text{--}500^\circ\text{C}$ below the dwell temperature have been identified as suitable slow-cooling periods, although many of the discussed compounds were prepared with no slow-cooling, thus it is not clear whether or not this is a necessary step in every synthesis. It is also worth noting that several of the synthetic procedures used to prepare the compounds discussed in this review include a multi-step temperature profile, in which the initial synthesis step involves slowly ramping to a given temperature and possibly dwelling at that temperature for some time, followed by quickly heating to the reaction temperature. This is a useful technique for reactions which contain reagents prone to decomposition or those which require a reaction of the starting materials prior to dissolving the reagents in the flux; for example, the decomposition of $\text{NH}_4\text{H}_2\text{PO}_4$ into a P_2O_5 flux or the pre-reaction of elemental sulfur or selenium with other reagents present in the reaction.

MATERIALS OBTAINED USING ABI FLUXES

By far the most numerous materials obtained from ABI fluxes are chalcogenides and oxychalcogenides, which comprise almost 50% of all phases (Figure 3). One of the main reasons for that is the suitability of the soft Pearson bases, bromide and iodide, to dissolve and provide a reaction medium for “soft” chalcogenides, whereas “harder” fluoride and chloride fluxes are more suitable for the oxide systems. There is however no strict boundary between the application of both types of fluxes and sometimes they can be used interchangeably. Another reason is that many research groups, once they found suitability of a certain flux for a system, tend to apply the same flux to all similar systems, which can also result in preference of some fluxes over other, although it does not necessarily mean that these phases could not be obtained by other fluxes.

OXIDES

The ABI fluxes have proved successful for the exploratory crystal growth of new complex oxides, where the bromides have

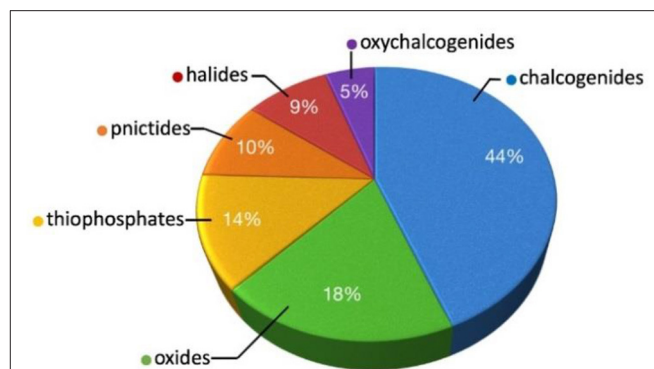


FIGURE 3 | An approximate distribution of the phases obtained using ABI fluxes.

received more attention compared to the iodides. In addition to exploratory crystal growth, the ABI fluxes have been used to recrystallize polycrystalline powders, control crystal morphology, and control structure compositions. The reactions generally consist of reacting the appropriate oxides, and in some cases the metal salts, with the ABI containing flux and heating the mixture to between 600 and 900°C for times ranging from a few hours to several days. CsBr was the most frequent flux used in oxide synthesis; in addition, several mixed fluxes were used including KCl/KI , NaBr/KBr , NaBr/CsBr , KI/KNO_3 , and the very complex $\text{NH}_4\text{Cl/AlF}_3/\text{NaCl/KBr/H}_3\text{BO}_3$ mixture.

CsBr has been extensively used as a flux by the Schleid group for the single crystal growth and structure determination of several families of rare earth selenates and silicates, namely $\text{MF}(\text{SeO}_3)$ ($M = \text{Sc, Y, Ho-Lu}$), $\text{Ho}_3(\text{SeO}_3)_4$, $\text{Sc}_2\text{O}_2(\text{SeO}_3)$, $\text{Er}_3\text{F}(\text{SiO}_4)_2(\text{SeO}_3)_2$, and $\text{Pr}_5(\text{SiO}_4)_2(\text{SeO}_3)_3$ (Wickleder et al., 2002; Lipp and Schleid, 2007, 2008a,b,c, 2009; Lipp et al., 2012, 2013; Chou et al., 2014; Greiner et al., 2017). The $\text{MF}(\text{SeO}_3)$ family features an unusual pentagonal bipyramidal coordination environment for the rare earth cation. Generally, the respective rare earth sesquioxide, rare earth fluoride, and SeO_2 were mixed in a 1:1:3 ratio with an excess amount of CsBr and heated in a carbon coated silica ampule at $700\text{--}850^\circ\text{C}$ for 5–7 days. In the case of the silicates, the silica tube reaction vessel acts as the SiO_2 source due to the reactive nature of fluorides toward the silica. Schleid used alumina crucibles or gold ampules contained within the silica tubes to protect the tube from the reactive fluoride.

The ABI fluxes have also been used to control the crystal morphology of several oxides such as $\text{NaNd}(\text{MoO}_4)_2$ (Liu et al., 2016), $\text{KEu}(\text{MoO}_4)_2$ (Wu et al., 2013), $\text{Li}_2\text{NiPO}_4\text{F}$ (Yamada et al., 2018), and NaNbO_3 (Hamilton et al., 2020). In each case the identity of the flux or the amount of flux played a significant role in the crystal morphology. For $\text{KEu}(\text{MoO}_4)_2$, stoichiometric amounts of K_2CO_3 , Eu_2O_3 , and MoO_3 were mixed with excess amounts of KCl or KBr flux and heated at $700\text{--}850^\circ\text{C}$ for 2–6 h in an alumina crucible. As the temperature increases, the morphology of the isolated crystals changes from undefined to rod-like and ultimately to octahedral. Reactions at 750°C were determined to be best for rod shaped crystals and

longer dwell times produced larger crystal sizes, while KBr was preferred over KCl, as it produced crystals more uniform in size (Wu et al., 2013).

Similarly, in the synthesis of $\text{NaNd}(\text{MoO}_4)_2$, the bromide flux resulted in a smaller distribution of crystal sizes. Crystals of $\text{NaNd}(\text{MoO}_4)_2$ were obtained with mixing Na_2CO_3 , Nd_2O_3 , and MoO_3 in stoichiometric amounts and adding excess amounts of NaCl or NaBr flux and heating the mixture in an alumina crucible at 750–900°C for 10 min to 6 h. In addition to the flux identity, the temperature and dwell time were important variables for control over the morphology of the crystals. Using a lower dwell temperature of 750°C produced crystals with no defined morphology, and as the temperature was increased more defined octahedral crystals were obtained. Larger crystals can be obtained

with longer dwell times, and the enhanced size of the crystals resulted in an increase of the emission peaks of the luminescent compound (Liu et al., 2016).

Crystals of $\text{Li}_2\text{NiPO}_4\text{F}$ were grown from mixtures of LiCO_3 , NiO, $\text{NH}_4\text{H}_2\text{PO}_4$ that were preheated at 400°C for 3 h before adding LiF and excess KCl/KI flux and heating the mixture to 600°C for 1 h. The morphology of the $\text{Li}_2\text{NiPO}_4\text{F}$ crystals was sensitive to the ratio of the preheated reactants and to the amount of KCl/KI flux (**Figure 4**). By increasing the amount of the flux, the morphology of the crystals changed from undefined to faceted, to rectangularly shaped, to one dimensional rods (Yamada et al., 2018).

A variety of fluxes were used for the synthesis of NaNbO_3 in order to determine the influence on particle size and morphology

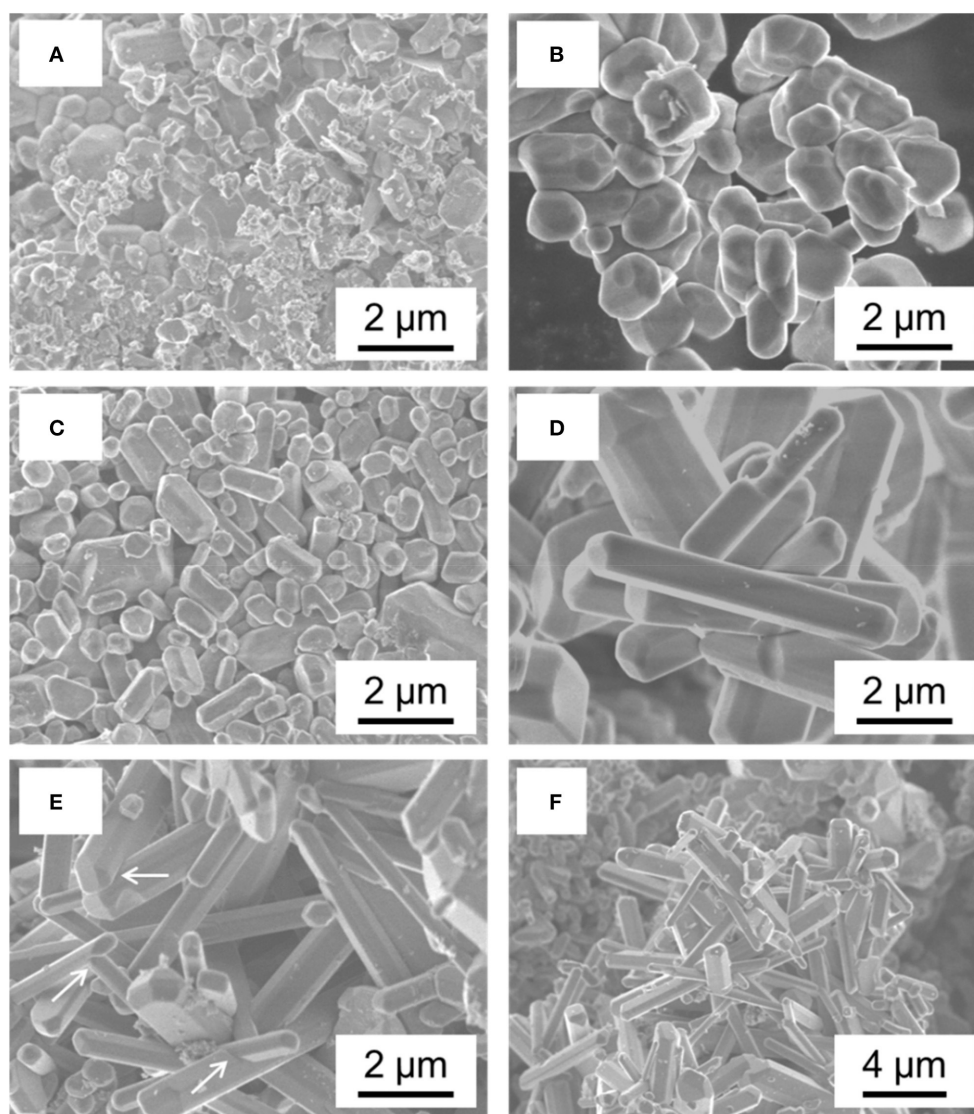


FIGURE 4 | SEM images of $\text{Li}_2\text{NiPO}_4\text{F}$ grown from KCl-KI fluxes showing the progression of crystal morphology as the mol % of reactants to flux decreases **(A)** 100, **(B)** 80, **(C)** 50, **(D)** 20, and **(E)** 10 mol %. **(F)** Lower magnification image of **(E)**. Reproduced from Yamada et al. (2018) with permission of American Chemical Society.

as well as photocatalytic activity. Out of the fluxes used (Na_2SO_4 , NaF , NaCl , and NaBr), NaBr produced the largest particles with the surface area of the particles was nearly twice as large as the next leading flux; however, photocatalytic activity was much higher in particles grown using Na_2SO_4 (Hamilton et al., 2020).

The successful synthesis of $\text{Sr}_3\text{MgSi}_2\text{O}_8:\text{Eu}^{2+}$ was also dependent on the ratio of the flux components. $\text{Sr}_3\text{MgSi}_2\text{O}_8:\text{Eu}^{2+}$ made by mixing SrCO_3 , MgO , SiO_2 , and Eu_2O_3 with varying ratios of a four or five component flux including, NH_4Cl , AlF_3 , NaCl , KBr , and H_3BO_3 . Multiple ratios were attempted to find favorable conditions for the doping of Eu^{2+} , and also the best conditions for maximized luminescence. The authors concluded that changing the concentrations of NH_4Cl and H_3BO_3 greatly influenced the luminescence of the products, where increasing NH_4Cl seemed to improve luminescence efficiency, while increasing the amount of H_3BO_3 had a negative impact on the efficiency; the relative amounts of NaCl and KBr did not play a significant role (Zhang et al., 2016).

The identity of the alkali halide flux was also used to control the doping of the alkali cation, and thus the oxidation of Mn, in Na and K doped LaMnO_3 . For both Na and K doped LaMnO_3 systems, La_2O_3 and MnCO_3 were added to the desired flux (Al, ABr, or AI) and heated at 900, 850, or 750°C, respectively (Shivakumara et al., 2001, 2004). In both systems, the doping of the alkali cation was most extensive in the AI flux, i.e., $\text{La}_{0.85}\text{Na}_{0.14}\text{MnO}_{2.97}$ (NaCl , 900°C), $\text{La}_{0.88}\text{Na}_{0.12}\text{Mn}_{0.96}\text{Na}_{0.04}\text{O}_3$ (NaBr , 850°C), and $\text{La}_{0.84}\text{Na}_{0.16}\text{Mn}_{0.93}\text{Na}_{0.07}\text{O}_3$ (NaI , 750°C) and $\text{La}_{0.85}\text{K}_{0.08}\text{MnO}_{2.93}$ (KCl , 900°C), $\text{La}_{0.89}\text{K}_{0.07}\text{MnO}_{2.99}$ (KBr , 800°C), and $\text{La}_{0.88}\text{K}_{0.10}\text{Mn}_{0.98}\text{O}_3$ (KI , 750°C). In the Na system, a small amount of Na was also doped on the Mn site if NaBr or NaI were used. In the K system, the more extensive doping of the K in the case of using a KI flux leads to a higher symmetry structure type. No discussion was given on how temperature influences the incorporation of Na or K, although different temperatures were chosen for the different fluxes.

In the study of the crystal growth of MgFe_2O_4 , MgAl_2O_4 , and MgCr_2O_4 the identity of the chosen flux was determined to have significant effects on the yield of the reaction. MgFe_2O_4 , MgAl_2O_4 , and MgCr_2O_4 can be synthesized by mixing MgO and the corresponding M_2O_3 with excess NaBr or KBr and heating in a platinum crucible. While both fluxes were effective at producing the desired product, using LiF or LiCl resulted in a higher yield as compared to NaBr and KBr (Yanagida and Atumi, 1967). ABI fluxes are also useful for recrystallizing powder products obtained from traditional solid state routes in order to obtain single crystals large enough for single crystal structure determination. For example, both $\text{Cs}_2\text{V}_4\text{O}_9$ and $\text{Rb}_2\text{V}_3\text{O}_8$ crystals were obtained in this manner using a CsBr or RbBr flux. Crystals of $\text{Cs}_2\text{V}_4\text{O}_9$ were grown by carrying out the solid state reaction with CsVO_3 and V_2O_3 in a sealed Pyrex tube at 550°C for 10 h, followed by mixing the resulting powder with a large excess of CsBr in a fused silica tube and heating at 700°C before slow cooling at 6°C/h to 470°C (Liu and Greedan, 1995). The crystal growth of $\text{Rb}_2\text{V}_3\text{O}_8$ was carried out in a similar manner, where stoichiometric ratios of RbVO_3 , V_2O_3 , and V_2O_5 are mixed and heated at 550°C overnight in a sealed tube, then the resulting powder is added to excess RbBr flux and heated in a sealed

fused silica tube to 750°C and slowly cooled to 500°C at 6°C/h (Liu and Greedan, 1995).

A number of complex metal oxides have been obtained from ABI fluxes, where the ABI flux plays an important role of providing alkali cations that incorporate into the final structure. Crystals of $\text{Cs}_2\text{Cu}_3\text{P}_4\text{O}_{10}$ were grown from CuO , P_2O_5 , and CsI flux in an evacuated fused silica tube heated at 700°C for 2 days followed by slow cooling to 300°C at 6°C/h (Sanjaya Ranmohotti et al., 2006). Similarly, NaCuAsO_4 was grown from the combination of As_2O_5 , CuO , CuBr_2 , and Cs_2O in an excess of eutectic NaBr/CsBr flux. Carbon coated silica ampules were used as the reaction vessel and heated to 300°C for 1 day, then 650°C for 4 days followed by slow cooling to 450°C at 2.5°C/h (Ulutagay-Kartin et al., 2003). To obtain crystals of $\text{Ba}_2\text{K}_2\text{Te}_2\text{O}_9$, $\text{Ba}(\text{H}_4\text{TeO}_6)$ was added in a 1:5 weight ratio with KNO_3/KI flux and heated in a platinum crucible to 500°C, held for 4 days, and slow cooled to room temperature in 12 h (Weil, 2018). The layered oxide, $\text{Na}_{0.27}\text{CoO}_2$, can be prepared by mixing $\text{CaC}_2\text{O}_4 \cdot 2\text{H}_2\text{O}$ with 10 times excess NaI and heating in an alumina crucible at 750°C for 24 h (Shivakumara and Hegde, 2003). Lastly, $\text{Cs}_3(\text{UO}_2)_2(\text{PO}_4)_2\text{O}_2$ can be obtained by loading a platinum crucible with $(\text{UO}_2)_3(\text{PO}_4)_2(\text{H}_2\text{O})_4$ and CsI flux and heating to 750°C for 10 h followed by slow cooling at 7°C/h to room temperature. The unique 3D framework contains larger pores filled with Cs cations (Yagoubi et al., 2013). On the contrary, the synthesis of $\text{Bi}_2(\text{Sr}_{1-x}\text{Ca}_x)_3\text{Cu}_2\text{O}_y$ gives an example of an unreactive flux. This composition was obtained from dissolving stoichiometric ratios of Bi, Sr, Ca, and Cu nitrates in water and heating up to 500°C and dwelling for 20 h before adding 75% by weight KBr flux and heating in a platinum crucible at 3 h followed by heating to 850 or 880°C and slow cooling to 700°C at 1°C/h (Shishido, 1990).

HALIDES/OXYHALIDES

There are about half as many halide containing phases grown from ABI fluxes as compared to oxide phases and the structures of the halide containing phases are highly varied and include simple binary phases, perovskite related, high order extended structures, and organic containing extended structures. As compared to the oxides, whose syntheses had a wide variety of mixed fluxes reported, almost all the oxyhalides are grown from single component melts.

Among the reported binary phases are $\text{Hf}_{0.86}\text{I}_3$ and $\text{TaBr}_{2.94}$ (Habermehl et al., 2010; Beekhuizen et al., 2011). Black rod-shaped crystals of $\text{Hf}_{0.86}\text{I}_3$ were produced by reducing HfI_4 with aluminum at 850°C in the presence of NaI flux contained in a sealed tantalum vessel and held for 16 days before slow cooling to room temperature at 5°C/h. The structure is composed of hexagonal close packed layers of iodide ions where 5.16 out of the 6 octahedral holes are filled by Hf ions (Beekhuizen et al., 2011). $\text{TaBr}_{2.94}$ completes the five-member family of binary tantalum bromides TaBr_5 , TaBr_4 , $\text{Ta}_6\text{Br}_{15}$, and $\text{Ta}_6\text{Br}_{14}$; the $\text{TaBr}_{2.94}$ structure is distantly related to the perovskite structure type. $\text{TaBr}_{2.94}$ was obtained by the reduction of TaBr_5 with the

wall of the tantalum reaction vessel at 500°C with NaBr or RbBr flux (Habermehl et al., 2010).

The ternary phases include Cs_2AuBr_6 , Cs_2AuI_6 , $\text{Y}_{16}\text{Br}_{24}\text{Ir}_4$, and the derivatives of the $\text{Ba}_7\text{F}_{12}\text{Cl}_2$ structure. Single crystals of the distorted perovskites, Cs_2AuBr_6 and Cs_2AuI_6 , were obtained from slow heating mixtures of Au, Br₂ or I₂, and CsI in alumina crucibles sealed inside fused silica tubes at 630 and 550°C, respectively over 42 h and dwelling for 10 h. After heating, the reactions were cooled at 5°C/h (Riggs et al., 2012). $\text{Y}_{16}\text{Br}_{24}\text{Ir}_4$ was obtained in a good yield using Ir metal, YBr_3 , and a RbI or KI flux and heating in a sealed Nb tube at 900°C for 5 weeks (Steinwand and Corbett, 1996). $\text{Ba}_{6.668}\text{Ca}_{0.332}\text{F}_{12}\text{Br}_2$ and the $\text{Ba}_{7-x}\text{Ca}_x\text{F}_{12}(\text{Cl}_y\text{Br}_{1-y})_2$ family both adopt the $\text{Ba}_7\text{F}_{12}\text{Cl}_2$ structure and were obtained from the appropriate alkaline earth halides and a NaBr or NaCl/NBr flux, respectively. The reactions were contained in covered platinum reaction vessels and heated to 900°C and cooled to 600°C in 3 h (Frühmann et al., 2004).

Further examples demonstrating the versatility of ABI fluxes include the novel lithium europium and strontium carbodiimides, $\text{LiSr}_2(\text{NCN})\text{I}_3$, $\text{LiEu}_2(\text{NCN})\text{I}_3$, and $\text{LiEu}_4(\text{NCN})_3\text{I}_3$, which resulted from a reaction of EuI_2 , NaCN, NaN_3 , and LiI (Liao et al., 2004a). The reactions were contained in sealed tantalum ampoules within sealed fused silica tubes and heated to 880°C [or 700°C for $\text{LiEu}_4(\text{NCN})_3\text{I}_3$] for 3 days and cooled at 6°C/min to room temperature. Both Eu containing compositions were obtained using the same ratio of reactants and the product identity was controlled by adjusting the temperature (Liao et al., 2004a). The presence of divalent europium in the structure was confirmed by magnetic measurements, with effective magnetic moments of 8.00(7) and 7.65(5) μ_B per Eu, respectively, within the expected range of magnetic moments for Eu^{2+} . $\text{LiSr}_2(\text{NCN})\text{I}_3$ features a unique extended structure with empty tetrahedral Sr_4 entities (Liao et al., 2004b). Crystals of the $\text{M}_6\text{N}_3\text{S}_4\text{Br}$ ($\text{M} = \text{La} - \text{Nd}$) compounds were grown from oxidizing the rare earth metal with sulfur and NaN_3 with the corresponding MBr_3 in the presence of a NaBr flux. The reactions were heated at 850°C for 7 days in evacuated silica tubes (Lissner and Schleid, 2002).

The reported synthetic conditions for obtaining halides, so far, have not used any metal oxide starting materials, but rather used metals in their elemental forms, likely to prevent the inclusion of O in the resulting structures. Two of the three oxyhalides use oxide precursors, while the oxygen source for $((\text{C}_2)_2\text{O}_2\text{Dy}_{14})\text{I}_{24}$ is not discussed. $\text{La}_3\text{OBr}(\text{AsO}_3)_2$ was synthesized from heating stoichiometric mixtures of $\text{NH}_4\text{H}_2\text{AsO}_4$, NH_4Br , and La_2O_3 in platinum crucibles at 500°C for 6 h and 850°C for 60 h before adding 20 equivalents of NaBr/KBr flux and heating at 900°C for 72 h and slow cooling at 10°C/h to room temperature (Yahia et al., 2010). In the synthesis of the oxyhalide, $\text{CsSm}_{21}(\text{SeO}_3)_{24}\text{Br}_{16}$, SmOBr and SeO_2 , were reacted in a CsBr flux and heated at 797°C and slow cooled to 570 K at 5°C/h (Ruck and Schmidt, 2003). Crystals of the oxyhalide $((\text{C}_2)_2\text{O}_2\text{Dy}_{14})\text{I}_{24}$, were synthesized from DyI_3 , Dy powder, graphite powder, and NaI flux using a He-arc sealed tantalum reaction vessel heated at 1,000°C for 10 days; however, the source of O in the structure was not discussed (Daub and Meyer, 2010).

CHALCOGENIDES

Binaries

ABI fluxes were employed to synthesize or recrystallize several binary chalcogenide compounds. In order to obtain new, non-linear optical materials, Zhang et al. performed a reaction between Ga_2O_3 , S, and B at 950°C (Zhang et al., 2013). In the absence of a flux, the reaction resulted in monoclinic Ga_2S_3 , whereas the addition of KI flux favored the formation of a cubic polymorph. Both compounds show a good Second Harmonic Generation (SHG) response and an exceptional laser induced damage threshold (LIDT). These two reactions are good examples of how a flux can divert a reaction pathway and lead to a different product, emphasizing the importance of new flux applications to known systems to discover new phases.

The application of different fluxes and the use of different flux to reagent ratios can also help fine tune the particle size of binary chalcogenides. For example, ZnS:Cu, Al phosphor particle sizes can be optimized by controlling the identity and the amount of the flux (Kawai et al., 1981). Interestingly, fluxes like NaCl and CaCl_2 facilitate a fast initial particle growth followed by virtually no further size increase with time, whereas CsCl, KCl, KI, and NaI fluxes behaved in a similar way except they promoted a secondary particle growth step after the plateau time. Another example of a flux controlled particle size synthesis is growth of CoS_2 particles in KCl, KBr, and KI fluxes (Figure 5; Wang et al., 2012). In the absence of a flux, the reaction between stoichiometric amounts of Co and S resulted in particles with an irregular morphology, while the flux reactions resulted in faceted, polyhedral particles. Among the three fluxes, the KCl flux was found to provide the most uniform sized polyhedra.

Large single crystals of PdS for electrical transport property measurements were grown from a KI flux (Cao et al., 2018). A powder sample of PdS was initially obtained by reacting stoichiometric quantities of the elements at 900°C and then recrystallized from a 20-fold excess of KI at the same temperature,

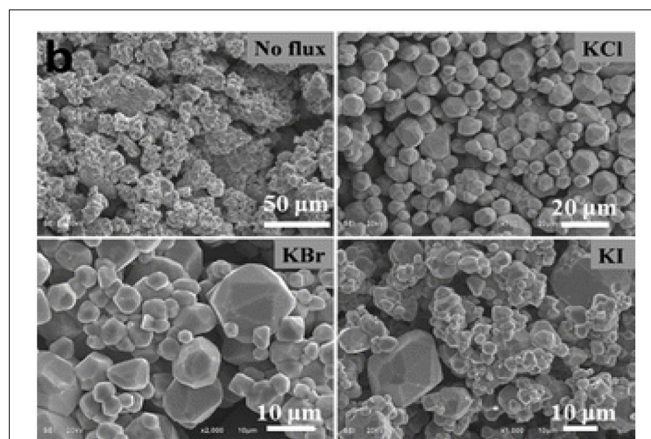


FIGURE 5 | The influence of different fluxes on the size and shape of CoS_2 particles. Reproduced from Wang et al. (2012) with permission of American Chemical Society.

demonstrating the ability of the KI flux to dissolve sulfide materials. The same flux has been used to obtain single crystals of PrS_2 at a temperature of 700°C , slightly above the flux melting point of 681°C (Vasilyeva and Belaya, 1999). A KBr flux allowed for the crystallization of $\text{SmTe}_{1.80}$ single crystals from a mixture of the elements; however, no efforts were made to improve upon the relatively low 5% yield of the phase (Ijjaali and Ibers, 2006). As a final example, it was determined that SnS could be recrystallized as a single phase from a KI flux at 740°C (Timmo et al., 2016).

Mixed Chalcogenides

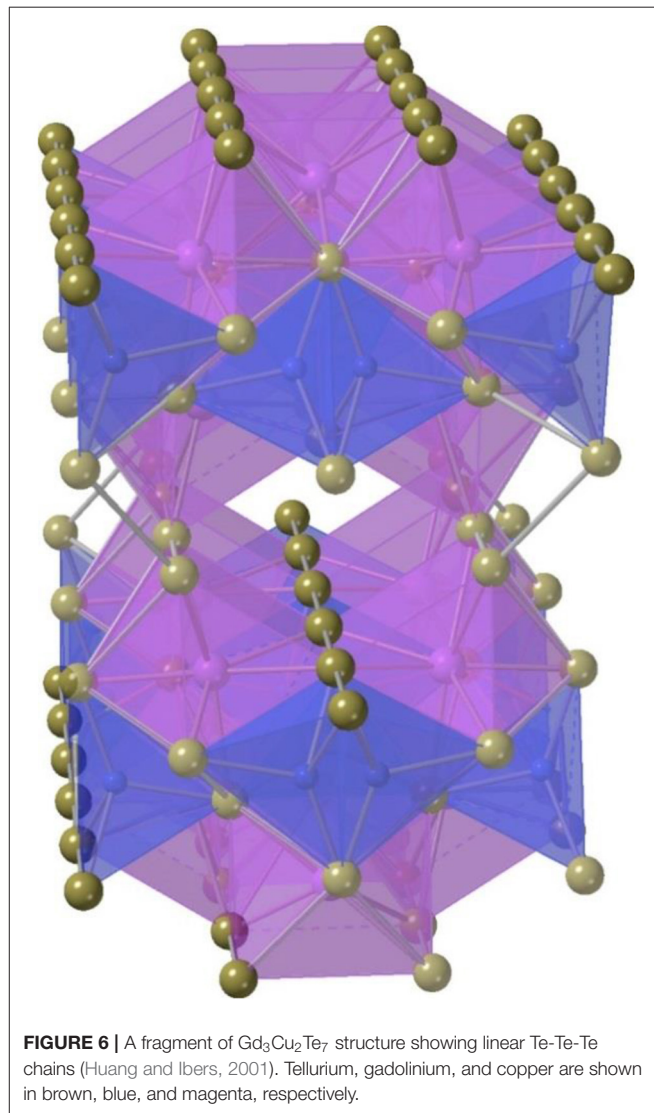
The ABI fluxes can offer a convenient reaction media to obtain mixed chalcogenide phases, such as $\text{Nd}_2\text{S}_2\text{Te}$, $\text{Dy}_4\text{S}_4\text{Te}_3$, $\text{CsTb}_3\text{STe}_4$, and $\text{CsTb}_5\text{S}_2\text{Te}_6$. The latter two compounds were crystallized from a CsBr flux at 850°C via the oxidation of Tb metal with S and Te (Lissner et al., 2019). At the same temperature, the direct reaction of Nd, Se, and Te in a stoichiometric ratio resulted in $\text{Nd}_2\text{S}_2\text{Te}$ powder, which can be recrystallized in an equimolar amount of CsBr flux (Schleid and Klein, 2001). A ternary mixed chalcogenide phase $\text{Dy}_4\text{Se}_4\text{Te}_3$ has been obtained starting with Dy_2O_3 and B as a reducing agent in a KI flux (Guo and Guo, 2014). A similar composition with very similar unit cell metrics, $\text{Dy}_4\text{S}_4\text{Te}_{2.3}$, was obtained by the reaction between Dy_2S_3 , Dy_2Te_3 , and Te.

Ternaries

A number of ternary phases have been obtained from the ABI fluxes. For example, colorless single crystals of Li_3AsS_3 were grown from a LiI flux starting with the elements. Although the melting point of LiI is about 469°C , the crystals were successfully grown at 450°C , indicating a possible reaction between the flux and the starting materials led to a melting point lowering of the flux (Huber et al., 2012). A reactive NaBr flux at 950°C was used to produce single crystals of NaIn_3S_5 from CaS and In_2S_3 (Zeng et al., 2015). In this reaction the flux provides both a reaction medium and functions as the Na^+ source. Another antimony ternary chalcogenide, Ni_2SbTe_2 , was obtained by reacting stoichiometric ratios of the elements in a KI flux at 900°C (Reynolds et al., 2004). The same reaction in the absence of the flux resulted in a product with the same composition, however in the form of smaller single crystals. Babo et al. reported on the synthesis of the ternary tellurides RbSc_5Te_8 , KYTe_2 , and RbYTe_2 that were prepared using KBr and RbBr as reactive fluxes at 900°C (Babo and Schleid, 2008, 2009). A study on the crystal growth of photoluminescent $\text{Pb}_2\text{P}_2\text{S}_6$ in KI at 800°C and LiBr/KBr at 500°C fluxes revealed different particle morphologies of the final products as a function of the flux used (Zhang et al., 2014). This serves as a good illustration of how different flux choices (and reaction temperatures) can be used to tune particle size and optical properties of the resulting material.

There are several lanthanide chalcogenide systems that were explored using ABI fluxes (Prakash et al., 2016), and the synthesis of new *f*-element chalcogenides tends to attract a lot of attention because of their interesting structural features and magnetic and optical properties (Bugaris and Ibers, 2010). For example, the structures of $\text{Gd}_3\text{Cu}_2\text{Te}_7$ and $\text{U}_2\text{Cu}_{0.78}\text{Te}_6$, which were both isolated from a KI flux at 850°C , contain

linear Te-Te chains (Figure 6), a common structural motif in chalcogenide chemistry (Huang and Ibers, 2001). Numerous compositions can be obtained from ABI fluxes, for example, a large family of lanthanide copper sulfides, LnCuQ_2 (Ln = lanthanides, Q = S, Se), was synthesized using several different flux systems. Successful crystal growth in this system was achieved with CsCl, KBr, and KI fluxes (Ijjaali et al., 2004; Strobel et al., 2005; Strobel and Schleid, 2007), where, interestingly, KBr and KI are interchangeable for the recrystallization of LnCuSe_2 (La, Ce, Pr, Nd, and Sm) (Ijjaali et al., 2004). An isotopic series of composition RbLnSe_2 was prepared from a RbI flux using an excess of Rb_2S_3 , which potentially also functioned as an auxiliary flux. Most *f*-elements are magnetic and due to the localized nature of the *4f* electrons, RbCeSe_2 , RbTbSe_2 , and RbErSe_2 exhibit simple paramagnetic behavior with no apparent magnetic interaction between the lanthanide cations. A Curie-Weiss law fit for RbCeSe_2 shows a large



negative Weiss constant, which was attributed to crystal-field splitting of the $^2F_{5/2}$ Ce(III) ground state (Deng et al., 2002).

The ABI fluxes allow for the synthesis of compounds containing both $3d$ and $4f$ elements as well as interlanthanide phases, which can result in interesting physical properties due to interactions between the metal cations. For example, a series of compounds Ln_3TSe_6 ($Ln = Sm, Gd$; $T = In, Cr$) and Tb_3CrSe_6 were obtained by reacting stoichiometric quantities of the elements in a KBr flux at $850^\circ C$ (Tougait and Ibers, 2000a). The products exhibit magnetic properties and magnetic measurements on Gd_3CrSe_6 revealed a sharp drop in the magnetic susceptibility below 10(1) K, indicative of an antiferromagnetic transition. No such drop in the susceptibility was observed for the analogous Sm_3CrSe_6 and Tb_3CrSe_6 compositions, suggesting that the ordering originates from the Gd^{3+} cations. Related mixed $4f$ element chalcogenides, Er_3SmQ_6 ($Q = S, Se$) and $Er_{1.12}Sm_{0.88}Se_3$, were grown from a KI flux (Gray et al., 2007). Although the structures of Er_3SmQ_6 ($Q = S, Se$) exhibit minimal Er/Sm disorder as they are found in different coordination environments with coordination numbers of 6 and 7 for Er and 8 for Sm, it is difficult to precisely quantify the amount of disorder as their X-ray scattering is very similar.

Quaternaries

The ABI fluxes often provide alkali cations that incorporate into the final products, thus playing the role of a reactive flux. This incorporation favors more complex compositions that usually result in more complex crystal structures. A number of non-centrosymmetric quaternary chalcogenide phases have been reported and were investigated for their non-linear optical properties. For example, by exploiting the lone pair effect of Sb^{3+} to induce non-centrosymmetry, La_2CuSbS_5 was synthesized in a mixed CsBr/BaCl₂ flux at $900^\circ C$ (Lin et al., 2019). This compound exhibits a reasonable SHG response ($0.5 \times AgGaS_2$) with a large LIDT ($6.7 \times AgGaS_2$). Another couple of NLO active sulfides, $Ba_4CuGa_5Q_{12}$ ($Q = S, Se$), were grown from a KBr flux at $750^\circ C$ (Kuo et al., 2013), and their SHG response demonstrated that the sulfide compound is a promising NLO material in infrared region. Further improvements of the optical characteristics were observed in $Ba_{10}Zn_7M_6Q_{26}$ ($M = In, Ga$; $Q = S, Se$) that were obtained by a reaction of the elements in a KBr/CsBr flux confined in a graphite crucible at $1,000^\circ C$ (Li et al., 2018). Similarly, single crystals of $Ba_6Zn_6ZrS_{14}$ were grown by the direct combination of the elements in the presence of a KI flux at $900^\circ C$ (Bezuidenhout et al., 2014). The product mixture contained Ba_2ZnS_3 as a side product, and optimization of the solid state reaction condition was able to yield a phase pure sample starting from the elements. The product is stable against water exposure and exhibits good photoluminescent properties that make it a possible candidate for optical applications.

Quaternary lanthanide chalcogenides have been studied extensively for their magnetic properties and several series of compounds have been crystallized out of ABI fluxes. Yao et al. prepared KLn_2CuS_4 ($Ln = Y, Nd, Sm, Tb, Ho$) and $K_2Ln_4Cu_4S_9$ ($Ln = Dy, Ho$) by the reactive flux method using K_2S and KI to aid crystal growth at $700^\circ C$ (Yao et al., 2003).

All compounds can also be obtained in the absence of KI, however with significantly lower yields. Magnetic measurements performed on $K_2Ho_4Cu_4S_9$ showed a paramagnetic behavior with a magnetic moment that agrees well with the theoretical value of $10.60 \mu_B$ for Ho^{3+} . Two other copper-containing phases, $SrCuCeSe_3$ and $SrCuPrSe_3$, were obtained from CsI flux at $800^\circ C$ (Strobel and Schleid, 2004). Despite the very similar sizes of the lanthanide cations in these two compounds, they adopt distinct structure types.

The use of a KBr/BaBr₂ mixed flux enables Ba incorporation into the final product as can be illustrated by the synthesis of the quaternary chalcogenides $BaLnMQ_3$ ($Ln =$ lanthanide, $M = Cu, Ag, Au$, $Q = Se$ or Te) (Yang and Ibers, 1999). The Ln and M elements along with BaQ were mixed with a KBr/BaBr₂ flux and reacted at $850^\circ C$. The flux-assisted reactions yielded single crystals in 35–65% yield with minor quantities of Ln_2Q_3 impurities, while only binaries of Ln/Te formed in similar reactions without a flux. Inverse magnetic susceptibility data for $BaNdAgTe_3$ were fitted to a Curie-Weiss law, and exhibit no magnetic transitions down to 5 K. In a similar way, $Ba_4Nd_2Cd_3Se_{10}$ and $Ba_4Ln_2Cd_3S_{10}$ ($Ln = Sm, Gd, Tb$) were formed from a BaBr₂/KBr flux at $900^\circ C$ (Yang and Ibers, 2000). The reciprocal magnetic susceptibility of the Tb-containing compound was fit to the Curie-Weiss law and resulted in an effective magnetic moment of $9.94 \mu_B$, which is consistent with the theoretical value of $9.72 \mu_B$.

The KBr flux offers a convenient way to synthesize pentanary $KCaEr_2CuS_5$, providing both solution for crystal growth and the K^+ cation that incorporates into the structure (Zeng et al., 2006). Initially, a mixture of Er_2S_3 , CaS, Cu, and S were employed as starting materials. However, while optimizing the reaction conditions it was determined that an optimal yield is obtained when Cu_2S is used instead of a mixture of the elements. The compound exhibits paramagnetic behavior down to 5 K and an estimated bandgap of 2.4 eV measured by UV-vis spectroscopy.

Thiophosphates and Thiosilicates

The ABI fluxes have been used to prepare several families of thiophosphate compounds. Isostructural $K_{0.5}Ag_{0.5}Nb_2PS_{10}$ and $Rb_{0.38}Ag_{0.5}Nb_2PS_{10}$ were grown from the elements in eutectic AgI/KI and AgI/RbI fluxes, respectively, at $800^\circ C$ (Dong et al., 2005; Dong Y. et al., 2005). Similarly, KBr and CsBr fluxes at $950^\circ C$ were used to obtain $Rb_3Ln_3[PS_4]_4$ ($Ln = Pr, Er$) and $Cs_3Pr_5[PS_4]_6$ (Komm and Schleid, 2004, 2005). Crystal growth of rare earth sulfides $NaLnP_2S_6$ ($Ln = La$ and Ce) and $CsLnP_2S_7$ ($Ln = Pr, Nd, Sm, Gd, Tb, Dy, Ho, Er, Yb$, and Y) was facilitated by a CsI/NaI flux at $500^\circ C$ (Klepov et al., 2019a). The synthesis of the $NaLnP_2S_6$ compounds is preceded by reduction of the P(V) containing P_2S_5 starting material to P(IV) in $P_2S_6^{4-}$. Possible reducing agents for this reaction are iodide and sulfide anions, although it is unclear which anion contributes more. Magnetic susceptibility measurements revealed paramagnetic behavior of all compounds and the effective moments derived from Curie-Weiss law fits are in a good agreement with the expected theoretical values. In a similar way, uranium thiophosphates

were grown from eutectic CsI/NaI and RbI/NaI fluxes from US_2 , Na_2S , and P_2S_5 binaries at temperatures between 500 and 750°C (Klepov and zur Loye, 2018). All compounds exhibit rather complex compositions, $Cs_5Na_6[U(PS_4)_4](PS_4)$, $Rb_5Na_3[U(PS_4)_4]$, $CsNa[U(PS_4)_2]$, $Cs_{1.67}Na_{0.52}I_{0.19}[U(PS_4)_2]$, $Cs_{1.033}Na_{1.343}I_{0.376}[U(PS_4)_2]$, and $Rb_{1.35}Na_{0.93}I_{0.28}[U(PS_4)_2]$, and structures. Magnetic susceptibility data for $CsNa[U(PS_4)_2]$ indicate the transition from one paramagnetic state to another at 200–225 K, which is not accompanied with a structural change and is likely due to an electronic phenomenon.

There are several thiosilicates that were obtained from ABI fluxes. The serendipitous crystal growth of $NaY_3S_3[SiS_4]$ occurred when Be, Y, and S were reacted in an excess of a NaBr flux inside an evacuated silica tube, which served as a source of Si (Hartenbach and Schleid, 2003). The reaction was then optimized by using SiS_2 as a starting material in the same NaBr flux at 850°C, which resulted in a water- and air-resistant product in an approximate yield of 80%. Uranium(IV) thiosilicates $Cs_2Na_4[U_2(SiS_4)_2(Si_2S_8)]$ and $Cs_{2.12}Na_{3.88}[U_2(SiS_4)_2(Si_2S_7)]$ can be obtained from CsI and CsI/NaI eutectic fluxes by reacting US_2 , SiS_2 , and Na_2S (Klepov et al., 2019b). The reaction yielded phase pure $Cs_2Na_4[U_2(SiS_4)_2(Si_2S_8)]$, which exhibits paramagnetic properties as revealed by magnetic susceptibility measurements.

OXYCHALCOGENIDES

The ABI fluxes have also been employed to synthesize a variety of oxychalcogenide compounds. These are predominately oxyselenides (Tougait and Ibers, 2000b,c, 2001; Nitsche et al., 2014; Liu et al., 2015; Peschke et al., 2015, 2017a,b; Peschke and Johrendt, 2016, 2017), but also include oxysulfides (Zeng et al., 1999, 2002; Huang et al., 2000; Chi et al., 2016), and oxytellurides (Liu et al., 2007). In many cases, the ABI flux is utilized as a recrystallizing agent. For example, single crystals of $Ln_{3.67}Ti_2O_3Se_6$ ($Ln = Ce, Nd, Sm$) were grown by mixing a powdered sample of the material, synthesized from stoichiometric quantities of Ln, TiO_2 , Ti, and Se, with KBr in a fused silica tube. The reaction was heated to 950°C for 96 h before being slow cooled to room temperature (Tougait and Ibers, 2000c). In other cases, the materials are synthesized via the traditional flux method, where a combination of metal oxides and metal chalcogenides and/or elemental species, are combined with an ABI flux in an evacuated fused silica tube. $La_5Cu_6O_4S_7$ was grown in this way from a mixture of La_2S_3 , CuO, and KI flux heated to 900°C for 4 d and slow cooled to 300°C at a rate of 3°C/h (Huang et al., 2000). Similarly, $La_6Ti_3O_5Se_9$ was grown from a mixture of La, Ti, TiO_2 , Se, and KI flux heated to 950°C for 100 h and slow cooled to 700°C at a rate of 3°C/h (Tougait and Ibers, 2001).

In most cases, the oxychalcogenide material is formed by adding a limited, typically stoichiometric, amount of oxygen, in the form of a metal oxide precursor, into the evacuated fused silica tube. However, in the case of $Ln_4S_3Si_2O_7$, the oxygen was obtained from the reaction attacking the fused silica tube (Zeng

et al., 1999, 2002). These reactions utilized a KBr flux, as opposed to the alkali iodides that are used for the synthesis of most of the other oxychalcogenide systems, which is the likely cause of the fused silica etching. In a few other cases, an overstoichiometry of oxygen is used in combination with boron metal as an oxygen getter. For example, $BaGeOSe_2$ was synthesized from a mixture of Ba, GeO_2 , Se, B, and KI flux. In this reaction, the excess oxygen associated with the GeO_2 is captured by the boron metal to form B_2O_3 as a side product (Liu et al., 2015).

The synthesized oxychalcogenides have been explored for two primary purposes. Due to the different size and electronegativity of oxygen vs. chalcogenides, cationic oxychalcogenide polyhedra possess a larger polarity than their pure oxide counterparts. This can lead to increased second-harmonic generation when the oxychalcogenide crystallizes in a non-centrosymmetric space group. This is evident in non-centrosymmetric $BaGeOSe_2$, whose GeO_2Se_2 and $BaOSe_6$ polyhedra have dipole moments with magnitude 11.25 and 20.47, respectively. These are considerably greater than the moments of 4.65 and 4.70 for the respective pure oxide polyhedra and result in $BaGeOSe_2$ having a similar strength SHG response as $AgGaS_2$, a commercially used NLO crystal (Liu et al., 2015). A second interest in the oxychalcogenides arose from the discovery of high temperature superconductivity in the iron arsenides. As a result, considerable attention has been paid to structurally related rare-earth transition metal oxychalcogenides, for example, $RE_2FeSe_2O_2$ ($RE = La, Ce$) (Nitsche et al., 2014).

PNICTIDES

Ternaries

The use of ABI fluxes has also resulted in a number of pnictide phases exhibiting unique structural features, further demonstrating the versatility of the alkali bromide and iodide flux systems. As an example, Lissner and Schleid employed a CsBr flux in reactions of lanthanide metal powders, sulfur, cesium azide, and lanthanide tribromides at 900°C to obtain single crystals of $Ln_4N_2S_3$ ($Ln = La-Nd$) (Lissner and Schleid, 2006, 2017). It was noted that the four structures, which are isotypic to one another, exhibit an elongated Ln-S bond and an increase in the Ln(2) site coordination number from 6 to 6+1 along the series from La to Ce, an observation which diverges from expectations based on the lanthanide contraction. The authors later used similar methods to obtain the Ln_3NS_3 ($Ln = La-Nd, Sm, Gd-Dy$) series from a NaBr flux (Lissner et al., 2006). Schurz et al. obtained the first gadolinium nitride selenides, Gd_3NSE_3 and $Gd_{23}N_5Se_{27}$, by replacing sulfur with selenium and using gadolinium triiodide with a CsI flux (Schurz et al., 2013). A distinctive feature in the structure of $Gd_{23}N_5Se_{27}$ is the presence of gadolinium cations with a coordination number of 5, significantly lower in coordination than what is typically observed in lanthanide solid-state structures (Figure 7), which was attributed to the short coordinating anion bond distances of 2.20 Å for Gd(4)-N(1) and 2.77 Å for Gd(4)-Se(27).

In an effort to prepare new low-dimensional materials for semiconductor applications, Na_2BP_2 , a novel boron phosphide

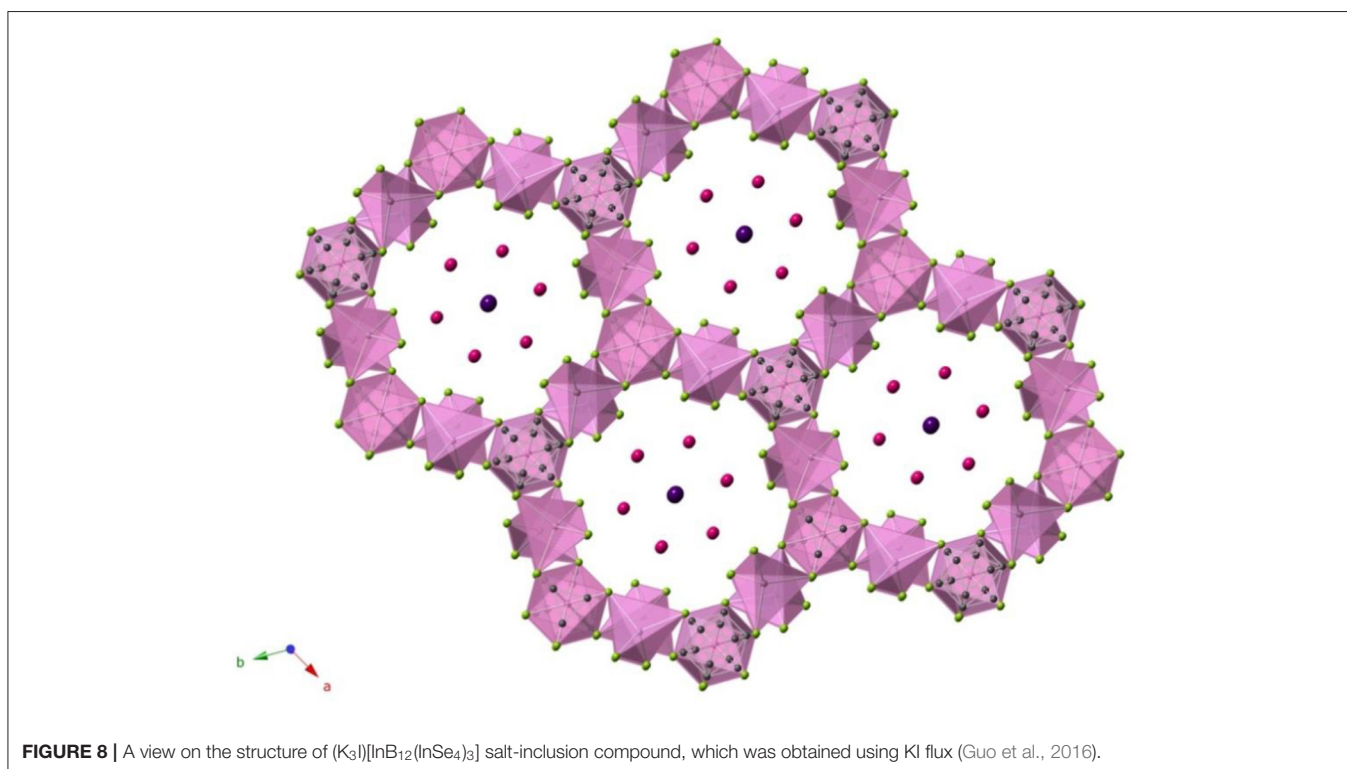
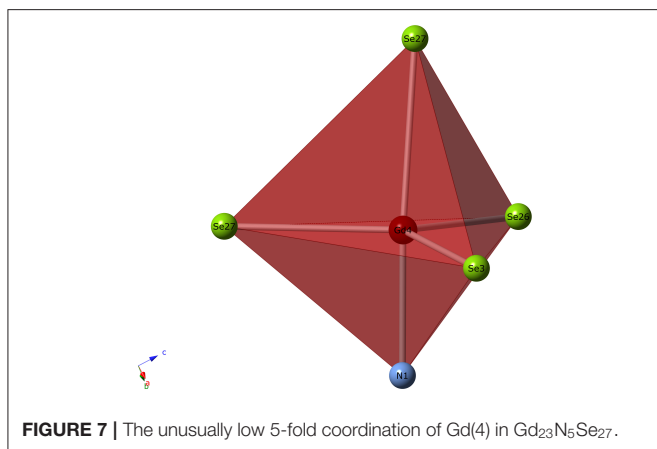
containing one-dimensional B-P chains was prepared (Woo et al., 2019). To avoid formation of inert and thermodynamically-favored phases, Woo et al. utilized mild reaction temperatures and oxidative elimination to prepare single crystals of the metastable Na_2BP_2 phase from a mixture of Na_3BP_2 and CuI in a CsI-NaI eutectic that was heated to 500°C . The authors suggested that this method may also offer a route to multidimensional materials by increasing the degree of oxidation. Using similar methods, Aydemir et al. serendipitously obtained $\text{Eu}_3[\text{B}_3\text{N}_6]$, the first entirely europium(III) nitridoborate (Aydemir et al., 2016). This phase was initially prepared from a NaBr flux and formed as a minor phase due to an EuBr_3 impurity in

the starting materials; it was surmised that the decomposition of EuBr_3 into EuBr_2 and Br_2 resulted in the oxidation step which yielded the product. This hypothesis was confirmed by heating a mixture of a divalent europium precursor $\text{Eu}_3[\text{BN}_2]_2$ and Br_2 to 800°C , yielding a mixture of $\text{Eu}_3[\text{B}_3\text{N}_6]$ and EuBr_2 (Aydemir et al., 2016).

Quaternaries

As opposed to the ternary pnictides, there have been only a few reports on the use of ABI fluxes to prepare quaternary pnictide phases. While combinations of lanthanide metal powder, sulfur or selenium, cesium azide, and lanthanum tribromides resulted in several ternary phases [$\text{Ln}_4\text{N}_2\text{S}_3$ ($\text{Ln} = \text{La-Nd}$), Gd_3NSe_3 , and $\text{Gd}_{23}\text{N}_5\text{Se}_{27}$], replacement of cesium azide with sodium azide resulted in the quaternary phase $\text{Nd}_3\text{N}_2\text{SeBr}$ (Lissner and Schleid, 2007), an outcome that emphasizes the importance in the choice of starting materials.

For photoelectrochemical water splitting applications, particles of SrNbO_2N were pre-calcined and heated in a variety of alkali halide fluxes; it was determined that SrNbO_2N particles flux-treated in NaI yielded the highest photocurrent density of 1.5 mA cm^{-2} at $1.23 \text{ V}_{\text{RHE}}$ under AM 1.5 G irradiation (Kodera et al., 2016). In the search for potential superconductors, LnFeAsO ($\text{Ln} = \text{La-Nd, Sm, Gd-Tb}$) has been studied, and was prepared by Nitsche et al. from a mixture of FeO , As , and lanthanide metal in a NaI-KI flux at $1,050^\circ\text{C}$ (Nitsche et al., 2010). Similar methods were later used to produce large single crystals of LaFeAsO from a KI flux, which were isolated as plates having an edge length of up to 1 mm (Jesche et al., 2012).



SALT-INCLUSION MATERIALS

Salt-inclusion materials (SIMs) represent a unique class of hierarchical materials that typically exhibit porous and covalent frameworks with interpenetrating ionic salt lattices. As functional materials, SIMs have wide-ranging applications as waste storage and ion exchange materials to optical materials. The zur Loye group has focused on synthesizing novel uranium-containing SIMs via alkali halide fluxes and while the majority of these have been prepared from ACI-AF eutectics, some success was achieved with the use of ABI fluxes. A novel intergrowth uranyl silicate, $K_8(K_5F)U_6Si_8O_{40}$, was grown from a KF-KBr flux (Morrison et al., 2016b), and unlike many other

uranyl compounds, $K_8(K_5F)U_6Si_8O_{40}$ was found to exhibit intense luminescence behavior possibly attributable to the salt-inclusion. Similarly, a KF-KBr flux was used to prepare $[KK_6Br_{0.6}F_{0.4}][[(UO_2)_3(Ge_2O_7)_2]]$ (Juillerat et al., 2018) in a study to explore the adaptability of the uranyl germanate SIM framework. This $[(UO_2)_3(Ge_2O_7)_2]$ framework was found to successfully accommodate twelve different salt-inclusions that were incorporated based on the selected flux used in the synthesis.

In addition to uranium-containing SIMs, ABI fluxes have demonstrated moderate success in stabilizing non-uranium SIMs as well. For example, the pentanary selenide $(K_3I)[InB_{12}(InSe_4)_3]$ was synthesized from a KI flux (Guo et al., 2016). The crystal

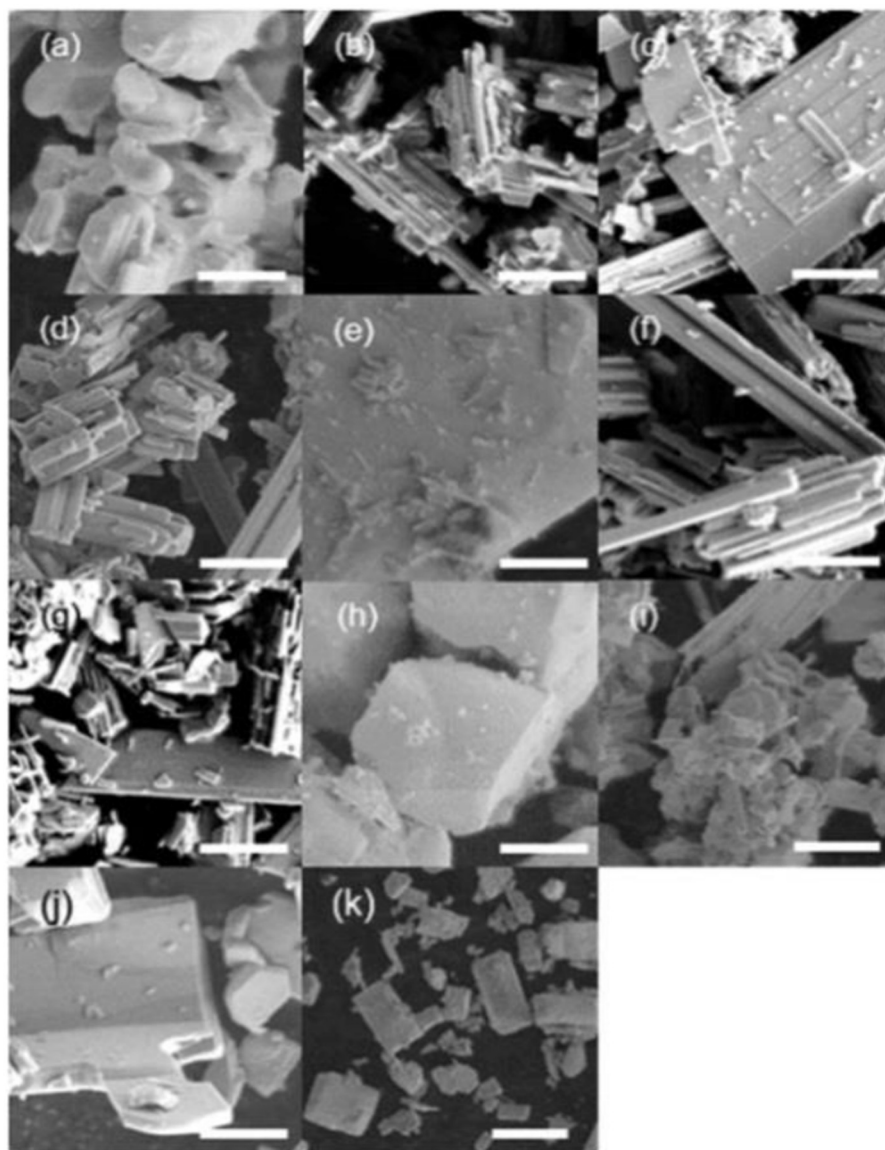


FIGURE 9 | SEM images of oxide precursors produced (a) without flux, and with (b) NaCl, (c) KCl, (d) RbCl, (e) $SrCl_2$, (f) NaBr, (g) KBr, (h) NaI, (i) KI, (j) CsI, and (k) $SrCl_2$ fluxes. The scale bars in (a–j) are 2 μm , and that in (k) is 20 μm . Reproduced from Kodera et al. (2016) under the Creative Commons CCBY-NC license—published by the Royal Society of Chemistry.

- Bale, C. W., Bélisle, E., Chartrand, P., Deckerov, S. A., Eriksson, G., Gheribi, A. E., et al. (2016). FactSage thermochemical software and databases, 2010–2016. *Calphad* 54, 35–53. doi: 10.1016/j.calphad.2016.05.002
- Bale, C. W., Bélisle, E., Chartrand, P., Deckerov, S. A., Eriksson, G., Hack, K., et al. (2009). FactSage thermochemical software and databases — recent developments. *Calphad* 33, 295–311. doi: 10.1016/j.calphad.2008.09.009
- Bale, C. W., Chartrand, P., Deckerov, S. A., Eriksson, G., Hack, K., Mahfoud, R. B., et al. (2002). FactSafe thermochemical software and databases. *Calphad* 26, 189–228. doi: 10.1016/S0364-5916(02)00035-4
- Beekhuizen, J., Mudring, A.-V., and Meyer, G. (2011). Linear trimeric hafnium clusters in $\text{Hf}_{0.86(1)}\text{I}_3$. *Cryst.* 1, 40–46. doi: 10.3390/cryst1020040
- Bezuidenhout, D. I., van der Westhuizen, B., Swarts, P. J., Chatturgoon, T., Munro, O. Q., Fernández, I., et al. (2014). Redox behaviour of cymantrene Fischer carbene complexes in designing organometallic multi-tags. *Chem. - Eur. J.* 20, 4974–4985. doi: 10.1002/chem.201304711
- Bugaris, D. E., and Ibers, J. A. (2010). Syntheses and characterization of some solid-state actinide (Th, U, Np) compounds. *Dalton Trans.* 39, 5925–6128. doi: 10.1039/b927026d
- Bugaris, D. E., and zur Loye, H.-C. (2012). Materials discovery by flux crystal growth: quaternary and higher oxides. *Angew. Chem. Int. Ed.* 51, 3780–3811. doi: 10.1002/anie.201102676
- Cao, L., Lv, Y.-Y., Chen, S.-S., Li, X., Zhou, J., Yao, S.-H., et al. (2018). Crystal growth and magneto-transport behavior of $\text{PdS}_{1-\delta}$. *J. Cryst. Growth* 487, 116–119. doi: 10.1016/j.jcrysgro.2018.02.026
- Chi, Y., Guo, S.-P., Kong, H.-J., and Xue, H.-G. (2016). Crystal and electronic structures, and optical and magnetic properties of novel rare-earth sulfide borates $\text{RE}_3\text{S}_3\text{BO}_3$ (RE = Sm, Gd). *New J. Chem.* 40, 6720–6727. doi: 10.1039/C6NJ00549G
- Chou, S.-C., Greiner, S., Magdysyuk, O. V., Dinnebier, R. E., and Schleid, T. (2014). Theoretical and experimental analysis of structural phase transitions for $\text{ScF}[\text{SeO}_3]$ and $\text{YF}[\text{SeO}_3]$. *Z. Anorg. Allg. Chem.* 640, 3203–3211. doi: 10.1002/zaac.201400287
- Cortese, A. J., Wilkins, B., Smith, M. D., Morrison, G., and zur Loye, H.-C. (2015). Single crystal growth and characterization of the first reduced lanthanum molybdenum oxychloride, $\text{La}_{20}\text{Mo}_{12}\text{O}_{63}\text{Cl}_4$, with an unusual trigonal prismatic MoO_6 unit. *Solid State Sci.* 48, 133–140. doi: 10.1016/j.solidstatesciences.2015.07.015
- Daub, K., and Meyer, G. (2010). Isolated and edge-connected tetramers $\{(\text{C}_2)_2\text{O}_2\text{Dy}_{14}\}$ in the crystal structures of $\{(\text{C}_2)_2\text{O}_2\text{Dy}_{14}\}\text{I}_{24}$ and $\{(\text{C}_2)_2\text{O}_2\text{Dy}_{12}\}\text{I}_{18}$. *Z. Anorg. Allg. Chem.* 636, 1716–1719. doi: 10.1002/zaac.201000128
- Deng, B., Ellis, D. E., and Ibers, J. A. (2002). New layered rubidium rare-earth selenides: syntheses, structures, physical properties, and electronic structures for RbLnSe_2 . *Inorg. Chem.* 41, 5716–5720. doi: 10.1021/ic020324j
- Dong, Y., Kim, S., and Yun, H. (2005). A new thiophosphate, $\text{Rb}_{0.38}\text{Ag}_{0.5}\text{Nb}_2\text{PS}_{10}$. *Acta Cryst. C* 61, i25–i26. doi: 10.1107/S0108270105000351
- Dong, Y.-K., King, S.-R., Yun, H.-S., and Lim, H.-J. (2005). Synthesis and crystal structure of a new pentanary thiophosphate, $\text{K}_{0.5}\text{Ag}_{0.5}\text{Nb}_2\text{PS}_{10}$. *Bull. Korean Chem. Soc.* 26, 309–311. doi: 10.5012/bkcs.2005.26.2.309
- Ferreira, T., Xing, J., Sanjeeva, L. D., and Sefat, A. S. (2020). Frustrated magnetism in triangular lattice TlYbS_2 crystals grown via molten flux. *Front. Chem.* 8:127. doi: 10.3389/fchem.2020.00127
- Frühmann, B., Kubel, F., Hagemann, H., and Bill, H. (2004). Synthesis and structure of the new fluoride bromide $\text{Ba}_{6.668(2)}\text{Ca}_{0.332(2)}\text{F}_{12}\text{Br}_2$ and solid solutions with composition $\text{Ba}_{6-x}\text{Ca}_x\text{F}_{12}(\text{Cl}_y\text{Br}_{1-y})_2$ with $x \approx 0.5$, $0 < y < 1$. *Z. Anorg. Allg. Chem.* 630, 1484–1488. doi: 10.1002/zaac.200400108
- Gouëlo, M., Hokkinen, J., Kärkelä, T., and Auvinen, A. (2018). A scoping study of the chemical behavior of cesium iodide in the presence of boron in the condensed phase (650°C and 400°C) under primary circuit conditions. *Nucl. Technol.* 203, 66–84. doi: 10.1080/00295450.2018.1429111
- Gray, D. L., Rodriguez, B. A., Chan, G. H., Van Duyne, R. P., and Ibers, J. A. (2007). Synthesis and characterization of Er_3SmQ_6 (Q=S, Se) and $\text{Er}_{1.12}\text{Sm}_{0.88}\text{Se}_3$. *J. Solid State Chem.* 180, 1527–1532. doi: 10.1016/j.jssc.2007.01.039
- Greiner, S., Chou, S.-C., and Schleid, T. (2017). Two anionically derivatized scandium oxoselenates(IV): $\text{ScF}[\text{SeO}_3]$ and $\text{Sc}_2\text{O}_2[\text{SeO}_3]$. *J. Solid State Chem.* 246, 160–166. doi: 10.1016/j.jssc.2016.11.011
- Guo, S.-P., and Guo, G.-C. (2014). Crystal structure and magnetic and photocatalytic properties of a new ternary rare-earth mixed chalcogenide, $\text{Dy}_4\text{S}_4\text{Te}_3$. *J. Mater. Chem. A* 2, 20621–20628. doi: 10.1039/C4TA04757E
- Guo, S. P., Chi, Y., Liu, B. W., and Guo, G. C. (2016). Synthesis, crystal structure and second-order nonlinear optical property of a novel pentanary selenide $(\text{K}_3\text{I})[\text{InB}_{12}(\text{InSe}_4)_3]$. *Dalton Trans.* 45, 10459–10465. doi: 10.1039/C6DT01602B
- Guo, S. P., Guo, G. C., Wang, M. S., Zou, J. P., Xu, G., Wang, G.-J., et al. (2009). A series of new infrared NLO semiconductors, $\text{ZnY}_6\text{Si}_2\text{S}_{14}$, $\text{Al}_x\text{Dy}_3\text{Si}_y\text{Al}_{1-y}\text{S}_7$, and $\text{Al}_{0.33}\text{Sm}_3\text{SiS}_7$. *Inorg. Chem.* 48, 7059–7065. doi: 10.1021/ic802443n
- Habermehl, K., Mudring, A.-V., and Meyer, G. (2010). The last of the five: the elusive “tantalum(III) bromide”, a perovskite-related salt, $[\text{Ta}_6\text{Br}_{12}]\text{Br}_3[\text{TaBr}_6]_{0.86}$. *Eur. J. Inorg. Chem.* 2010, 4075–4078. doi: 10.1002/ejic.201000581
- Hamilton, A. M., O'Donnell, S., Zoellner, B., Sullivan, I., and Maggard, P. A. (2020). Flux-mediated synthesis and photocatalytic activity of NaNbO_3 particles. *J. Am. Ceram. Soc.* 103, 454–464. doi: 10.1111/jace.16765
- Hartenbach, I., and Schleid, T. (2003). $\text{NaY}_3\text{S}_3[\text{SiS}_4]$: a sodium-containing yttrium sulfide thiosilicate with channel structure. *J. Solid State Chem.* 171, 382–386. doi: 10.1016/S0022-4596(02)00217-7
- Huang, F. Q., Brazis, P., Kannewurf, C. R., and Ibers, J. A. (2000). Synthesis, structure, electrical conductivity, and band structure of the rare-earth copper oxychalcogenide $\text{La}_5\text{Cu}_6\text{O}_4\text{S}_7$. *J. Solid State Chem.* 155, 366–371. doi: 10.1006/jssc.2000.8926
- Huang, F. Q., and Ibers, J. A. (2001). $\text{Gd}_3\text{Cu}_2\text{Te}_7$ and $\text{U}_2\text{Cu}_{0.78}\text{Te}_6$: two examples of linear Te chains. *J. Solid State Chem.* 159, 186–190. doi: 10.1006/jssc.2001.9149
- Huber, S., Preitschaft, C., Wehrich, R., and Pfitzner, A. (2012). Preparation, crystal structure, electronic structure, impedance spectroscopy, and raman spectroscopy of Li_3SbS_3 and Li_3AsS_3 . *Z. Anorg. Allg. Chem.* 638, 2542–2548. doi: 10.1002/zaac.201200277
- Ijjaali, I., and Ibers, J. A. (2006). Two new binary lanthanide polytellurides: Syntheses and crystal structures of $\text{CeTe}_{1.90}$ and $\text{SmTe}_{1.80}$. *J. Solid State Chem.* 179, 3456–3460. doi: 10.1016/j.jssc.2006.07.010
- Ijjaali, I., Mitchell, K., and Ibers, J. A. (2004). Preparation and structure of the light rare-earth copper selenides LnCuSe_2 (Ln=La, Ce, Pr, Nd, Sm). *J. Solid State Chem.* 177, 760–764. doi: 10.1016/j.jssc.2003.09.007
- Jesche, A., Nitsche, F., Probst, S., Doert, T., Müller, P., and Ruck, M. (2012). Anisotropic electrical resistivity of LaFeAsO : evidence for electronic nematicity. *Phys. Rev. B* 86, 134511. doi: 10.1103/PhysRevB.86.134511
- Juillera, C. A., Klepov, V. V., Morrison, G., Pace, K. A., and zur Loye, H.-C. (2019). Flux crystal growth: a versatile technique to reveal the crystal chemistry of complex uranium oxides. *Dalton Trans.* 48, 3162–3181. doi: 10.1039/C8DT04675A
- Juillera, C. A., Moore, E. E., Morrison, G., Smith, M. D., Besmann, T. M., and zur Loye, H.-C. (2018). Versatile uranyl germanate framework hosting twelve different alkali halide 1D salt inclusions. *Inorg. Chem.* 57, 11606–11615. doi: 10.1021/acs.inorgchem.8b01729
- Kanatzidis, M. G. (2017). Discovery-synthesis, design, and prediction of chalcogenide phases. *Inorg. Chem.* 56, 3158–3173. doi: 10.1021/acs.inorgchem.7b00188
- Kanatzidis, M. G., Pöttgen, R., and Jeitschko, W. (2005). The metal flux: a preparative tool for the exploration of intermetallic compounds. *Angew. Chem.* 44, 6996–7023. doi: 10.1002/anie.200462170
- Kanatzidis, M. G., and Sutorik, A. C. (1995). The application of polychalcogenide salts to the exploratory synthesis of solid state multinary chalcogenides at intermediate temperatures. *Progr. Inorganic Chem.* 43, 151–265. doi: 10.1002/9780470166444.ch2
- Kawai, H., Abe, T., and Hoshina, T. (1981). Effects of fluxes on junction growth of ZnS phosphor. *Jpn. J. Appl. Phys.* 20, 313–320. doi: 10.1143/JJAP.20.313
- Kishimoto, M., Latif, H., Kita, E., and Yanagihara, H. (2017). Characterization of FeCo particles synthesized via co-precipitation, particle growth using flux treatment and reduction in hydrogen gas. *J. Magn. Magn. Mater.* 432, 404–409. doi: 10.1016/j.jmmm.2016.12.078
- Klepov, V. V., Breton, L. S., Pace, K. A., Kocovski, V., Besmann, T. M., and zur Loye, H.-C. (2019a). Size-driven stability of lanthanide

- thiophosphates grown from an iodide flux. *Inorg. Chem.* 58, 6565–6573. doi: 10.1021/acs.inorgchem.9b00806
- Klepov, V. V., Smith, M. D., zur Loye, H.-C. (2019b). Targeted Synthesis of Uranium(IV) Thiosilicates. *Inorg. Chem.* 58, 8275–8278. doi: 10.1021/acs.inorgchem.9b01307
- Klepov, V. V., and zur Loye, H.-C. (2018). Complex topologies from simple building blocks: uranium(IV) thiophosphates. *Inorg. Chem.* 57, 11175–11183. doi: 10.1021/acs.inorgchem.8b01733
- Kodera, M., Urabe, H., Katayama, M., Hisatomi, T., Minegishi, T., and Domen, K. (2016). Effects of flux synthesis on SrNbO₂N particles for photoelectrochemical water splitting. *J. Mater. Chem. A*, 4, 7658–7664. doi: 10.1039/C6TA00971A
- Komm, T., and Schleid, T. (2004). The new cesium praseodymium thiophosphate Cs₃Pr₅[PS₄]₆. *Z. Anorg. Allg. Chem.* 630, 712–716. doi: 10.1002/zaac.200400010
- Komm, T., and Schleid, T. (2005). The first rubidium rare-earth(III) thiophosphates: Rb₃M₃[PS₄]₄ (M=Pr, Er). *J. Solid State Chem.* 178, 454–463. doi: 10.1016/j.jssc.2004.07.048
- Kong, X., Lou, T., and Li, Y. (2005). Fe₇S₈ nanorods and nanosheets. *J. Alloys Compd.* 390, 236–239. doi: 10.1016/j.jallcom.2004.07.054
- Kuo, S.-M., Chang, Y.-M., Chung, I., Jang, J.-I., Her, B.-H., Yang, S.-H., et al. (2013). New metal chalcogenides Ba₄CuGa₅Q₁₂ (Q = S, Se) displaying strong infrared nonlinear optical response. *Chem. Mater.* 25, 2427–2433. doi: 10.1021/cm400311v
- Li, Y.-Y., Wang, H., Sun, B.-W., Ruan, Q.-Q., Geng, Y.-L., Liu, P.-F., et al. (2018). Ba₁₀Zn₇M₆Q₂₆: two new mid-infrared nonlinear optical crystals with T₂ supertetrahedron 3D framework. *Cryst. Growth Des.* 19, 1190–1197. doi: 10.1021/acs.cgd.8b01644
- Liao, W., Hu, C., Kremer, R. K., and Dronskowski, R. (2004a). Formation of complex three- and one-dimensional interpenetrating networks within carbodiimide chemistry: NCN⁻-coordinated rare-earth-metal tetrahedra and condensed alkali-metal iodide octahedra in two novel lithium europium carbodiimide iodides, LiEu₂(NCN)₃ and LiEu₄(NCN)₃I₃. *Inorg. Chem.* 43, 5884–5890. doi: 10.1021/ic049432r
- Liao, W., von Appen, J., and Dronskowski, R. (2004b). LiSr₂(NCN)₃: the first empty tetrahedral strontium(II) entity coordinated by carbodiimide units but without strontium–strontium bonding. *Chem. Commun.* 20, 2302–2303. doi: 10.1039/B408647C
- Lin, H., Li, Y.-Y., Li, M.-Y., Ma, Z., Wu, L.-M., Wu, X.-T., et al. (2019). Centric-to-acentric structure transformation induced by a stereochemically active lone pair: a new insight for design of IR nonlinear optical materials. *J. Mater. Chem. C*, 7, 4638–4643. doi: 10.1039/C9TC00647H
- Lipp, C., Burns, P. C., and Schleid, T. (2012). Pr₃F[SiO₄][SeO₃]₃: another complex fluoride oxosilicate oxoselenate(IV). *Z. Anorg. Allg. Chem.* 638, 779–784. doi: 10.1002/zaac.201100493
- Lipp, C., Dinnebie, R. E., and Schleid, T. (2013). LuF[SeO₃]: the structural chameleon of lanthanoid fluoride oxoselenates(IV). *Inorg. Chem.* 52, 10788–10794. doi: 10.1021/ic4006289
- Lipp, C., and Schleid, T. (2007). LuF[SeO₃] und LuCl[SeO₃]: Zweinicht-isotope Halogenid-oxoselenate(IV) des Lutetiums. *Z. Anorg. Allg. Chem.* 633, 1429–1434. doi: 10.1002/zaac.200700158
- Lipp, C., and Schleid, T. (2008a). Er₃F[SiO₄][SeO₃]₂: an ErF₃-derivative with two different kinds of complex oxoanions. *Z. Anorg. Allg. Chem.* 634, 1025–1029. doi: 10.1002/zaac.200700583
- Lipp, C., and Schleid, T. (2008b). Ein neues selten-erd-metall(III)-fluorid-oxoselenat(IV): YF[SeO₃]. *Z. Anorg. Allg. Chem.* 634, 657–661. doi: 10.1002/zaac.200700544
- Lipp, C., and Schleid, T. (2008c). HoF[SeO₃] und Ho₃F[SeO₃]₄: Zwei fluorid-derivatisierte oxoselenate(IV) des Holmiums. *Z. Anorg. Allg. Chem.* 634, 1662–1668. doi: 10.1002/zaac.200800099
- Lipp, C., and Schleid, T. (2009). The rare-earth metal(III) fluoride oxoselenates(IV) MF[SeO₃] (M = Y, Ho–Lu) with YF[SeO₃]-type structure. *Z. Naturforsch.* 64B, 375–382. doi: 10.1515/znb-2009-0403
- Lissner, F., Meyer, M., Kremer, R. K., and Schleid, T. (2006). M₃NS₃ (M = La–Nd, Sm, Gd–Dy): Struktur und Magnetismus von 3:1:3-Typ-Nitridsulfiden dreiwertiger Lanthanide. *Z. Anorg. Allg. Chem.* 632, 1995–2002. doi: 10.1002/zaac.200600159
- Lissner, F., Meyer, S. P., and Schleid, T. (2019). CsTb₃STe₄ und CsTb₅S₂Te₆: Zwei pseudo-ternäre caesium-terbium-chalkogenide mit geordneten S²⁻- und Te²⁻-Anionen. *Z. Naturforsch.* 74, 99–107. doi: 10.1515/znb-2018-0174
- Lissner, F., and Schleid, T. (2002). Nitridsulfidhalogenide der leichten Lanthanide vom Typ M₆N₃S₄X (M = La–Nd; X = Cl, Br) mit ausgeordneten Sulfid- und Halogenid-Lagen. *Z. Naturforsch.* 57b, 1079–1084. doi: 10.1515/znb-2002-1001
- Lissner, F., and Schleid, T. (2006). La₄N₂S₃: Ein neues Nitridsulfid des Lanthans mit beispielloser Kristallstruktur. *Z. Anorg. Allg. Chem.* 632, 1167–1172. doi: 10.1002/zaac.200500420
- Lissner, F., and Schleid, T. (2007). Nd₃N₂SeBr: Ein neues Nitridselenidbromid des Neodyms mit-Strängen aus hochkondensierten [NNd₄]⁹⁺-Tetraedern. *Z. Anorg. Allg. Chem.* 633, 1973–1978. doi: 10.1002/zaac.200700264
- Lissner, F., and Schleid, T. (2017). The A-type Ln₄N₂S₃ series: new nitride sulfides of the light lanthanoids (Ln = Ce–Nd). *Inorganics* 5:2. doi: 10.3390/inorganics5010002
- Liu, B.-W., Jiang, X.-M., Wang, G.-E., Zeng, H.-Y., Zhang, M.-J., Li, S.-F., et al. (2015). Oxychalcogenide BaGeOSe₂: highly distorted mixed-anion building units leading to a large second-harmonic generation response. *Chem. Mater.* 27, 8189–8192. doi: 10.1021/acs.chemmater.5b03649
- Liu, C., Liu, Y., Lyu, Y., and Lyu, C. (2016). Morphology and photoluminescence properties of NaNd(MoO₄)₂ synthesized by a molten salt method. *J. Mater. Sci. Mater. Electron.* 27, 5735–5740. doi: 10.1007/s10854-016-4486-5
- Liu, G., and Greedan, J. E. (1995). Magnetic properties of fersnoite-type vanadium oxides: A₂V₃O₈ (A = K, Rb, NH₄). *J. Solid State Chem.* 114, 499–505. doi: 10.1006/jssc.1995.1075
- Liu, M. L., Wu, L. B., Huang, F. Q., Chen, L. D., and Ibers, J. A. (2007). Syntheses, crystal and electronic structure, and some optical and transport properties of LnCuOTe (Ln=La, Ce, Nd). *J. Solid State Chem.* 180, 62–69. doi: 10.1016/j.jssc.2006.09.014
- Liu, X., Fechner, N., and Antonietti, M. (2013). Salt melt synthesis of ceramics, semiconductors and carbon nanostructures. *Chem. Soc. Rev.* 42, 8237–8265. doi: 10.1039/C3CS60159E
- Morrison, G., Smith, M. D., and zur Loye, H.-C. (2016a). Understanding the formation of salt-inclusion phases: an enhanced flux growth method for the targeted synthesis of salt-inclusion cesium halide uranyl silicates. *J. Am. Chem. Soc.* 138, 7121–7129. doi: 10.1021/jacs.6b03205
- Morrison, G., Tran, T. T., Halasyamani, P. S., and zur Loye, H.-C. (2016b). K₈(K₅F)U₆Si₈O₄₀: an intergrowth uranyl silicate. *Inorg. Chem.* 55, 3215–3217. doi: 10.1021/acs.inorgchem.6b00242
- Nitsche, F., Jesche, A., Hieckmann, E., Doert, T., and Ruck, M. (2010). Structural trends from a consistent set of single-crystal data of RFeAsO (R = La, Ce, Pr, Nd, Sm, Gd, and Tb). *Phys. Rev. B*, 82, 134514. doi: 10.1103/PhysRevB.82.134514
- Nitsche, F., Niklaus, R., and Johrendt, D. (2014). New polymorphs of RE₂FeSe₂O₂ (RE = La, Ce). *Z. Anorg. Allg. Chem.* 640, 2897–2902. doi: 10.1002/zaac.201400371
- Pace, K. A., Klepov, V. V., Morrison, G., and zur Loye, H.-C. (2018). Moderate supercritical synthesis as a facile route to mixed-valent uranium(IV,V) and (V,VI) silicates. *Chem. Commun.* 54, 13794–13797. doi: 10.1039/C8CC07789d
- Peschke, S., Gampel, L., Weippert, V., and Johrendt, D. (2017a). Flux synthesis, crystal structures, and physical properties of new lanthanum vanadium oxyselenides. *Dalton Trans.* 46, 6230–6243. doi: 10.1039/C7DT00779E
- Peschke, S., and Johrendt, D. (2016). The modulated structures of La_{2-x}Pr_xO₂MnSe₂ (0 ≤ x ≤ 1) and La_{2-x}Nd_xO₂MnSe₂ (0 ≤ x ≤ 0.6). *Zeitschrift für Kristallographie - Crystalline Materials* 231, 89–95. doi: 10.1515/zkri-2015-1883
- Peschke, S., and Johrendt, D. (2017). Flux synthesis, crystal structures, and magnetism of the series La_{2n+2}MnSe_{n+2}O_{2n+2} (n = 0–2). *Inorganics* 5:9. doi: 10.3390/inorganics5010009
- Peschke, S., Nitsche, F., and Johrendt, D. (2015). Flux synthesis, modulated crystal structures, and physical properties of REM_nO₅SeO (M = La, Ce). *Z. Anorg. Allg. Chem.* 641, 529–536. doi: 10.1002/zaac.201400603
- Peschke, S., Weippert, V., Senyshyn, A., Mühlbauer, M. J., Janka, O., Pöttgen, R., et al. (2017b). Flux synthesis, crystal structures, and magnetic ordering of the rare-earth chromium(II) oxyselenides RE₂CrSe₂O₂ (RE = La–Nd). *Inorg. Chem.* 56, 2241–2247. doi: 10.1021/acs.inorgchem.6b02895
- Prakash, J., Mesbah, A., Beard, J. C., Malliakas, C. D., and Ibers, J. A. (2016). Syntheses, crystal structures, and resistivities of the two new ternary

- uranium selenides, Er_3USe_8 and Yb_3USe_8 . *J. Solid State Chem.* 233, 90–94. doi: 10.1016/j.jssc.2015.10.003
- Read, C. M., Smith, M. D., and zur Loye, H.-C. (2015). Synthesis, crystal structure, and optical properties of a new complex uranium oxychloride. KUO_3Cl . *J. Chem. Cryst.* 45, 440–444. doi: 10.1007/s10870-015-0612-0
- Reynolds, T. K., Kelley, R. F., and DiSalvo, F. J. (2004). Electronic transport and magnetic properties of a new nickel antimonide telluride, Ni_2SbTe_2 . *J. Alloys Compd.* 366, 136–144. doi: 10.1016/j.jallcom.2003.07.008
- Riggs, S. C., Shapiro, M. C., Corredor, F., Geballe, T. H., Fisher, I. R., McCandless, G. T., et al. (2012). Single crystal growth by self-flux method of the mixed valence gold halides $\text{Cs}_2[\text{Au}^{\text{I}}\text{X}_2][\text{Au}^{\text{III}}\text{X}_4]$ ($\text{X}=\text{Br}, \text{I}$). *J. Cryst. Growth.* 355, 13–16. doi: 10.1016/j.jcrysgro.2012.06.039
- Ruck, M., and Schmidt, P. (2003). Synthesen und Kristallstrukturen der homöotypen selenitbromide $\text{Bi}_8(\text{SeO}_3)_9\text{Br}_6$ und $\text{CsSm}_{21}(\text{SeO}_3)_{24}\text{Br}_{16}$. *Z. Anorg. Allg. Chem.* 629, 2133–2143. doi: 10.1002/zaac.200300192
- Sanjaya Ranmohotti, K. G., Mo, X., Smith, M. K., and Hwu, S.-J. (2006). Synthesis, structure, and magnetic properties of $\text{Cs}_{2-x}\text{Rb}_x\text{Cu}_3\text{P}_4\text{O}_{14}$ ($0.0 \leq x \leq 0.8$): a new series of copper(II) phosphates containing periodic arrays of staggered square-planar CuO_4 trimers. *Inorg. Chem.* 45, 3665–3670. doi: 10.1021/ic060069t
- Schleid, T., and Klein, E. K. (2001). $\text{Nd}_2\text{S}_2\text{Te}$: Neodymium(III) sulfide telluride with $\text{Ce}_2\text{O}_2\text{S}$ -Type crystal structure. *Z. Anorg. Allg. Chem.* 627, 807–808. doi: 10.1002/1521-3749(200105)627:5<807::AID-ZAAC807>3.0.CO;2-R
- Schurz, C. M., Talmon-Gros, P., Lissner, F., and Schleid, T. (2013). The gadolinium nitride selenides Gd_3NSe_3 and $\text{Gd}_{23}\text{N}_5\text{Se}_{27}$: three connectivity types of $[\text{NGd}_4]^{9+}$ tetrahedra and fivefold coordinated Gd^{3+} cations. *Solid State Sci.* 17, 140–145. doi: 10.1016/j.solidstatesciences.2012.11.015
- Shi, Z., Xu, Z., Feng, J., Huang, H., Qian, Q., Yan, S., et al. (2018). Molten salt-assisted axis-oriented growth of Ta_3N_5 nanorod arrays with enhanced charge transport for efficient photoelectrochemical water oxidation. *CrystEngComm* 20, 5364–5369. doi: 10.1039/C8CE01016A
- Shishido, T. (1990). Growth and characterization of $\text{Bi}_2(\text{Sr}_{1-x}\text{Ca}_x)_3\text{Cu}_2\text{O}_y$ single crystals extracted from KBr flux. *Jpn. J. Appl. Phys.* 29, 2413–2414. doi: 10.1143/JJAP.29.2413
- Shivakumara, C., and Hegde, M. S. (2003). Low temperature synthesis of layered Na_xCoO_2 and K_xCoO_2 from NaOH/KOH fluxes and their ion exchange properties. *J. Chem. Sci.* 115, 447–457. doi: 10.1007/BF02708236
- Shivakumara, C., Hegde, M. S., and Subbanna, G. N. (2001). Low temperature synthesis of ferromagnetic $(\text{LaK})\text{MnO}_3$ from KCl , KBr and KI fluxes. *Solid State Sci.* 3, 43–48. doi: 10.1016/S1293-2558(00)01116-X
- Shivakumara, C., Subbanna, G. N., Lalla, N. P., and Hegde, M. S. (2004). Na substitution for La- and Mn-sites in LaMnO_3 from alkali halide fluxes: low temperature synthesis, structure and properties. *Mater. Res. Bull.* 39, 71–81. doi: 10.1016/j.materresbull.2003.09.027
- Steinwand, S. J., and Corbett, J. D. (1996). Oligomeric rare-earth-metal halide clusters. Three structures built of $(\text{Y}_6\text{Z}_4)\text{Br}_{36}$ Units ($\text{Z} = \text{Ru}, \text{Ir}$). *Inorg. Chem.* 35, 7056–7067. doi: 10.1021/ic960650x
- Strobel, S., Lauxmann, P., and Schleid, T. (2005). Münzmetall-lanthanid-chalkogenide: I. Kupfer(I)-Lanthanid(III)-Sulfide der Zusammensetzung CuMS_2 ($\text{M} = \text{La} - \text{Nd}, \text{Sm}, \text{Gd}, \text{Tb}$) im monoklinen A-Typ. *Z. Naturforsch.* 60b, 917–923. doi: 10.1515/znb-2005-0901
- Strobel, S., and Schleid, T. (2004). Quaternary strontium copper(I) lanthanoid(III) selenides with cerium and praseodymium: SrCuCeSe_3 and SrCuPrSe_3 , unequal brother and sister. *Z. Naturforsch.* 59b, 985–991. doi: 10.1515/znb-2004-0907
- Strobel, S., and Schleid, T. (2007). Münzmetall-lanthanid-chalkogenide: II. Kupfer(I)-Lanthanid(III) Sulfide der Zusammensetzung CuMS_2 ($\text{M} = \text{Dy} - \text{Lu}$) im orthorhombischen B-Typ. *Z. Naturforsch.* 62b, 15–22. doi: 10.1515/znb-2007-0103
- Timmo, K., Kauk-Kuusik, M., Pilvet, M., Mikli, V., Kärber, E., Raadik, T., et al. (2016). Comparative study of SnS recrystallization in molten CdI_2 , SnCl_2 and KI : comparative study of SnS recrystallization in molten CdI . *Phys. Status Solidi C* 13, 8–12. doi: 10.1002/pssc.201510082
- Tougait, O., and Ibers, J. A. (2000a). Ternary rare-earth selenides with the U_3ScS_6 structure type: synthesis, characterization, and some magnetic properties of Ln_3TSe_6 ($\text{Ln} = \text{Sm}, \text{Gd}$; $\text{T} = \text{In}, \text{Cr}$) and Tb_3CrSe_6 . *Inorg. Chem.* 39, 1790–1794. doi: 10.1021/ic9914802
- Tougait, O., and Ibers, J. A. (2000b). Gd_2OSe_2 . *Acta Cryst.* C56, 623–624. doi: 10.1107/S0108768100003025
- Tougait, O., and Ibers, J. A. (2000c). Synthesis and characterization of three new rare-earth titanium oxyselenides: $\text{Ln}_{3,67}\text{Ti}_2\text{O}_3\text{Se}_6$ ($\text{Ln} = \text{Ce}, \text{Nd}, \text{Sm}$). *Chem. Mater.* 12, 2653–2658. doi: 10.1021/cm000203m
- Tougait, O., and Ibers, J. A. (2001). Syntheses and crystal structures of the lanthanum titanium oxyselenides $\text{La}_4\text{Ti}_2\text{O}_4\text{Se}_5$ and $\text{La}_6\text{Ti}_3\text{O}_5\text{Se}_9$. *J. Solid State Chem.* 157, 289–295. doi: 10.1006/jssc.2000.9060
- Ulutagay-Kartin, M., Hwu, S.-J., and Clayhold, J. A. (2003). Nanostructured magnetic cuprate cluster: synthesis, structure, UV-Vis spectroscopy, and magnetic properties of a new copper(II) arsenate NaCuAsO_4 containing discrete $[\text{Cu}_4\text{O}_{16}]_2^{4-}$ clusters. *Inorg. Chem.* 42, 2405–2409. doi: 10.1021/ic026169q
- Vasilyeva, I. G., and Belaya, S. V. (1999). Sulfur nonstoichiometry of PrS_2 : a series of new sulfur-deficient phases. *J. Solid State Chem.* 146, 211–216. doi: 10.1006/jssc.1999.8335
- Wang, Y., Wu, J., Tang, Y., Lü, X., Yang, C., Qin, M., et al. (2012). Phase-controlled synthesis of cobalt sulfides for lithium ion batteries. *ACS Appl. Mater. Interfaces* 4, 4246–4250. doi: 10.1021/am300951f
- Weil, M. (2018). Crystal structures of the triple perovskites $\text{Ba}_2\text{K}_2\text{Te}_2\text{O}_9$, $\text{Ba}_2\text{KNaTe}_2\text{O}_9$, and redetermination of the double perovskite $\text{Ba}_2\text{CaTeO}_6$. *Acta Cryst.* E74, 1006–1009. doi: 10.1107/S2056989018009064
- Wells, D. M., Chan, G. H., Ellis, D. E., and Ibers, J. A. (2010). $\text{UTa}_2\text{O}(\text{S}_2)_3\text{Cl}_6$: A ribbon structure containing a heterobimetallic 5d-5f M_3 cluster. *J. Solid State Chem.* 183, 285–290. doi: 10.1016/j.jssc.2009.10.012
- Wickleder, C., Hartenbach, I., Lauxmann, P., and Schleid, T. (2002). $\text{Eu}_5\text{F}[\text{SiO}_4]_3$ und $\text{Yb}_5\text{S}[\text{SiO}_4]_3$: Gemischtvalente Lanthanoid-Silicate mit Apatit-Struktur Professor Welf Bronger zum 70. Geburtstag gewidmet. *Z. Anorg. Allg. Chem.* 628, 1602. doi: 10.1002/1521-3749(200207)628:7<1602::AID-ZAAC1602>3.0.CO;2-F
- Winiarski, M. J., Tran, T. T., Chamorro, J. R., and McQueen, T. M. (2019). $(\text{CsX})\text{Cu}_5\text{O}_2(\text{PO}_4)_2$ ($\text{X} = \text{Cl}, \text{Br}, \text{I}$): a family of Cu^{2+} $\text{S} = 1/2$ compounds with capped Kagomé networks composed of OCu_4 units. *Inorg. Chem.* 58, 4328–4336. doi: 10.1021/acs.inorgchem.8b03464
- Woo, K. E., Wang, J., Mark, J., and Kovnir, K. (2019). Directing boron-phosphorus bonds in crystalline solid: oxidative polymerization of $\text{P}=\text{B}=\text{P}$ monomers into 1D chains. *J. Am. Chem. Soc.* 141, 13017–13021. doi: 10.1021/jacs.9b06803
- Wu, T., Liu, Y., Lu, Y., Wei, L., Gao, H., and Chen, H. (2013). Morphology-controlled synthesis, characterization, and luminescence properties of $\text{KEu}(\text{MoO}_4)_2$ microcrystals. *CrystEngComm* 15, 2761–2768. doi: 10.1039/c3ce27073d
- Yagoubi, S., Renard, C., Abraham, F., and Obbade, S. (2013). Molten salt flux synthesis and crystal structure of a new open-framework uranyl phosphate $\text{Cs}_3(\text{UO}_2)_2(\text{PO}_4)_2$: spectroscopic characterization and cationic mobility studies. *J. Solid State Chem.* 200, 13–21. doi: 10.1016/j.jssc.2013.01.013
- Yahia, H. B., Rodewalk, U. C., and Pöttgen, R. (2010). Crystal structure of $\text{La}_3\text{OBr}[\text{AsO}_3]_2$. *Z. Naturforsch.* 65b, 1289–1292. doi: 10.1515/znb-2010-1018
- Yamada, T., Zetsu, N., Kim, H.-m., Hagano, Y., Handa, N., Yubuta, K., et al. (2018). One-dimensional growth of $\text{Li}_2\text{NiPO}_4\text{F}$ single crystals from intermediate LiNiPO_4 crystal surface using KCl - KI fluxes. *Cryst. Growth Des.* 18, 6777–6785. doi: 10.1021/acs.cgd.8b01031
- Yanagida, H., and Atumi, M. (1967). The effectiveness of alkali halide media for the process of MgFe_2O_4 formation. *J. Ceram. Assoc. Jpn.* 75, 349–352. doi: 10.2109/jcersj1950.75.868_349
- Yang, Y., and Ibers, J. A. (1999). Synthesis and characterization of a series of quaternary chalcogenides BaLnMQ_3 ($\text{Ln}=\text{Rare Earth}, \text{M}=\text{Coinage Metal}, \text{Q}=\text{Se or Te}$). *J. Solid State Chem.* 147, 366–371. doi: 10.1006/jssc.1999.8359
- Yang, Y., and Ibers, J. A. (2000). Syntheses and structures of the new quaternary compounds $\text{Ba}_4\text{Nd}_2\text{Cd}_3\text{Se}_{10}$ and $\text{Ba}_4\text{Ln}_2\text{Cd}_3\text{S}_{10}$ ($\text{Ln}=\text{Sm}, \text{Gd}, \text{Tb}$). *J. Solid State Chem.* 149, 384–390. doi: 10.1006/jssc.1999.8561
- Yao, J., Deng, B., Ellis, D. E., and Ibers, J. A. (2003). Syntheses, structures, physical properties, and electronic structures of KLn_2CuS_4 ($\text{Ln}=\text{Y}, \text{Nd}, \text{Sm}, \text{Tb}, \text{Ho}$) and $\text{K}_2\text{Ln}_4\text{Cu}_4\text{S}_9$ ($\text{Ln}=\text{Dy}, \text{Ho}$). *J. Solid State Chem.* 176, 5–12. doi: 10.1016/S0022-4596(03)00233-0
- Zeng, H.-Y., Mao, J.-G., Dong, Z.-C., Guo, G.-C., and Huang, J.-S. (2002). Synthesis and crystal structure of $\text{Ho}_4\text{S}_3\text{Si}_2\text{O}_7$. *Chin. J. Struct. Chem.* 21, 157–160.
- Zeng, H.-Y., Mao, J.-G., and Huang, J.-S. (1999). Synthesis and crystal structure of $\text{La}_4\text{S}_3\text{Si}_2\text{O}_7$. *J. Alloys Compd.* 291, 89–93. doi: 10.1016/S0925-8388(99)0292-3

- Zeng, H.-Y., Zhang, M.-J., Liu, B.-W., Ye, N., Zhao, Z.-Y., Zheng, F.-K., et al. (2015). NaIn_3S_5 , a new compound from the $\text{CaS-In}_2\text{S}_3/\text{NaBr}$ system. *J. Alloys Compd.* 624, 279–283. doi: 10.1016/j.jallcom.2014.11.039
- Zeng, H. Y., Mattausch, H., Simon, A., Zheng, F. K., Dong, Z. C., Guo, G. C., et al. (2006). $\text{KCaEr}_2\text{CuS}_5$: a new pentanary rare-earth layered chalcogenide without substitutional disorder. *Inorg. Chem.* 45, 7943–7946. doi: 10.1021/ic060907j
- Zeng, H. Y., Zheng, F. K., Guo, G. C., and Huang, J. S. (2008). Syntheses and single-crystal structures of $\text{La}_3\text{AgSnS}_7$, $\text{Ln}_3\text{M}_x\text{MS}_7$ ($\text{Ln} = \text{La, Ho, Er}$; $\text{M} = \text{Ge, Sn}$; $1/4 \leq x \leq 1/2$). *J. Alloys Compd.* 458, 123–129. doi: 10.1016/j.jallcom.2007.03.136
- Zhang, M.-J., Jiang, X.-M., Zhou, L.-J., and Guo, G.-C. (2013). Two phases of Ga_2S_3 : promising infrared second-order nonlinear optical materials with very high laser induced damage thresholds. *J. Mater. Chem. C.* 1:4754. doi: 10.1039/c3tc30808a
- Zhang, P., Chen, X., Zhang, Z., Fei, M., and Chen, L. (2016). Synthesis and photoluminescence of the blue phosphor $\text{Sr}_3\text{MgSi}_2\text{O}_8:\text{Eu}^{2+}$ optimized with the Taguchi method for application in near ultraviolet excitable white light-emitting diodes. *J. Lumin.* 169, 733–738. doi: 10.1016/j.jlumin.2015.05.003
- Zhang, X., He, J., Chen, W., Wang, C., Zheng, C., Lin, J., et al. (2014). Semiconductor $\text{Pb}_2\text{P}_2\text{S}_6$ and size-dependent band gap energy of its nanoparticles. *RSC Adv.* 4, 34288–34293. doi: 10.1039/C4RA06663D
- Zhu, X., Anzai, A., Yamamoto, A., and Yoshida, H. (2019). Silver-loaded sodium titanate photocatalysts for selective reduction of carbon dioxide to carbon monoxide with water. *Appl. Catal. B Environ.* 243, 47–56. doi: 10.1016/j.apcatb.2018.10.021

Conflict of Interest: The authors declare that the research was conducted in the absence of any commercial or financial relationships that could be construed as a potential conflict of interest.

Copyright © 2020 Klepov, Juillerat, Pace, Morrison and zur Loye. This is an open-access article distributed under the terms of the Creative Commons Attribution License (CC BY). The use, distribution or reproduction in other forums is permitted, provided the original author(s) and the copyright owner(s) are credited and that the original publication in this journal is cited, in accordance with accepted academic practice. No use, distribution or reproduction is permitted which does not comply with these terms.